Estimation of Impedance About the Human Elbow Joint Using the Surface Electromyogram

By
Karthik Krishna

A Thesis
Submitted to the Faculty
of the
Worcester Polytechnic Institute
In partial fulfillment of the requirements for the
Degree of Master of Science
in
Electrical Engineering
March 2005

_____
Prof. Edward A. Clancy
ECE Department,
Thesis Advisor

_____
Prof. Donald R. Brown
ECE Department,
Committee member

_____
Prof. Fred J. Looft
ECE Department
Committee member.

1 Abstract

In performing manual tasks, muscles are voluntarily contracted in order to produce force and orient the limb in the desired direction. Many occupational tasks are associated with frequent musculoskeletal disorders. In tasks involving skilful manipulation, very frequently the forces are focused on the upper limb and neck. Upper extremity cumulative trauma disorders are among the more common worker related injuries. These muscle disorders may be related to repetitive exertions, excessive muscle loads and extreme postures. One of the major challenges is to quantify the muscle load and researchers have tried various measures to quantify muscle load. Joint mechanical impedance can be a robust method to quantify muscle load. Joint mechanical impedance characterizes the dynamic torque-angle relationship of the joint. Joint impedance has been measured by earlier researchers, for limited tasks, by imparting force (or angle) perturbations on the joint and relating resultant angular (or force) changes. The joint impedance gives a quantitative measure related to muscle co-contraction level. Measurement of the mechanical impedance at the workplace may provide useful information relevant to the understanding of upper limb disorders.

Electromyogram (EMG) is the electrical activity of the muscle. Usually, an estimate of the EMG amplitude is obtained from the raw waveform recorded from the surface of the skin. EMG amplitude estimates can be used to non-invasively estimate torque about joints. Presently, there exists no means by which mechanical impedance can be estimated non-invasively (i.e., without external perturbations). Therefore, we proposed the use of EMG to noninvasively estimate the joint mechanical impedance. Our objective in this project was to determine the extent to which surface EMG can be used to estimate

mechanical impedance. Simulation studies were first performed to understand the extent to which this tool could be useful and to determine methods to be used for the experiment. The simulations were followed by evaluating and estimating mechanical impedance using data collected from one experimental subject.

Simulations helped to devise processing techniques for the measured signals and also to determine the length of data to be collected. Low pass filters for derivatives (used in the development of impedance estimates) were designed. Subtracting out a polynomial was the best approach to attenuate a low frequency drift (artifact) that occurs in torque measurements. Thirty seconds of data provided impedance estimates with a relative error of 5% when EMG amplitude estimates with SNR of 15 were used.

Experimental data from constant-posture, slowly force-varying background torque level showed that the elbow joint system behaved like a second order linear system between 2 Hz and 10 Hz. Co-contraction by subjects during experiments caused impedance estimates to be unexpectedly high even at low background torque. Further experiments would need to be conducted with the subjects being instructed to avoid co-contraction.

Acknowledgements

I am thankful to my advisor, Prof. Edward Clancy for all the guidance and support that he provided towards my thesis. I have learnt a great deal, while working with him on this research towards my Masters Degree.

I thank Prof. Denis Rancourt (University of Sherbrooke, Canada) for all his help towards the experimental data and apparatus. My acknowledgements to Prof. Fred Looft and Prof. Donald Brown for being on the thesis committee. I also thank Dean Daigneault for his help towards building the hardware for the EMG electrodes and signal conditioning circuit.

Table of Contents

Table of Figures

2 Introduction

Electromyography is the study of muscle function through the inquiry of the electrical signal the muscles emanate [6]. The surface electromyogram is the signal detected by an electrode on the surface of the skin. Researchers have been studying the relationship between the surface electromyogram (EMG) and torque produced about a joint as a means of estimating musculoskeletal load, in particular, and joint dynamics in general. Measurement and understanding of these dynamics is important in the prevention of musculoskeletal injuries at the work place, rehabilitation engineering and basic motor control research. A joint exhibits mechanical impedance since it produces a torque if it is subjected to a displacement. Joint mechanical impedance is a necessary property of the musculoskeletal system because it helps stabilize force interactive tasks like tool usage. Joint mechanical impedance can be modulated by co-contracting muscles about a joint [20]. For example, a worker using a power tool will co-contract his/her muscles to generate the mechanical impedance required to stabilize the tool. However excessive impedance may be associated with musculoskeletal injury.

Mechanical impedance has been measured for constant posture tasks and point-to-point motion tasks. These methods have not used EMG for estimating the impedance. In this project, we have estimated the joint mechanical impedance from surface EMG. This estimation process is similar to EMG-torque modeling.

EMG amplitude is defined as the time varying standard deviation of the surface EMG [11]. Surface EMG amplitude provides a measure of the muscular effort and also serves as an input to EMG-to-force models, myoelectric prosthesis, gait analysis, motion

control studies, and other applications [9]. There are various EMG processing techniques, some of which perform better than others and help reduce the amplitude estimate error.

Our aims in this project are to estimate the mechanical impedance of the elbow joint from surface EMG in a constant posture, slowly force varying task. One of the objectives is also to demonstrate through simulation that advanced methods of estimating surface EMG amplitude lead to better EMG-impedance estimates. The long-term objectives of this work would be to use EMG-based estimates of mechanical impedance to study mechanisms of musculoskeletal injury in occupation tasks.

Simulations were carried out to relate EMG amplitude to impedance using a second order linear model. Simulations give us useful insight about the kind of data that needed to be collected and the length of data to be collected in experimental studies. The length of data collected must be adequate for system identification, so that the impedance estimation is accurate. On the other hand, the duration of the data cannot be so long that the subject is under fatigue. EMG amplitudes are a noisy signal and therefore, the impedance estimates could be noisy and it would be useful to know the accuracy of estimation in the presence of noise. Our experiment involves a slowly varying operating point. Earlier experiments have been carried out using a constant operating point and simulations could provide information about system identification with a varying operating point. The contributions from this project are the simulations required to relate EMG to impedance and a preliminary examination and analysis of data collected from one subject.

3 Background

Surface electromyography is a technique used to record the electrical activity of skeletal muscles. As muscles are activated, they generate action currents that flow through the resistive medium of the tissues. The voltage gradients thus produced may be recorded as the myoelectric signal [1].

3.1 Physiological Basis of the Electromyogram

As shown in Figure 3-1c, the skeletal muscle is composed of muscle fibers. In most muscles, muscle fibers (or cells) extend over the length of the muscle and are attached to at least two different bones on either side by means of tendons [19]. Muscle fibers are made up of myofibrils. The muscle is surrounded by a tissue called fascia. A thin fibrous membrane that surrounds the muscle and separates it from other muscles is the fascia [2]. The deep surface of the fascia gives off septa (endomysium). The endomysium penetrate the muscle and provide connective and supportive structures to various subdivisions of the muscle.

The fasciculi (subdivision of the muscle), are surrounded by perimysium, a sheath formed by extensions of the fascia into the muscle. The surface of perimysium divides to yield septa that surround each muscle fiber. Each fasciculus as in Figure 3-1b can contain up to 150 muscle fibers. The endomysium, perimysium and epimysium (fascia) together serve two functions. First, at the end of the muscles the contractile portion gradually gives way to the connective tissue that blends with and becomes a

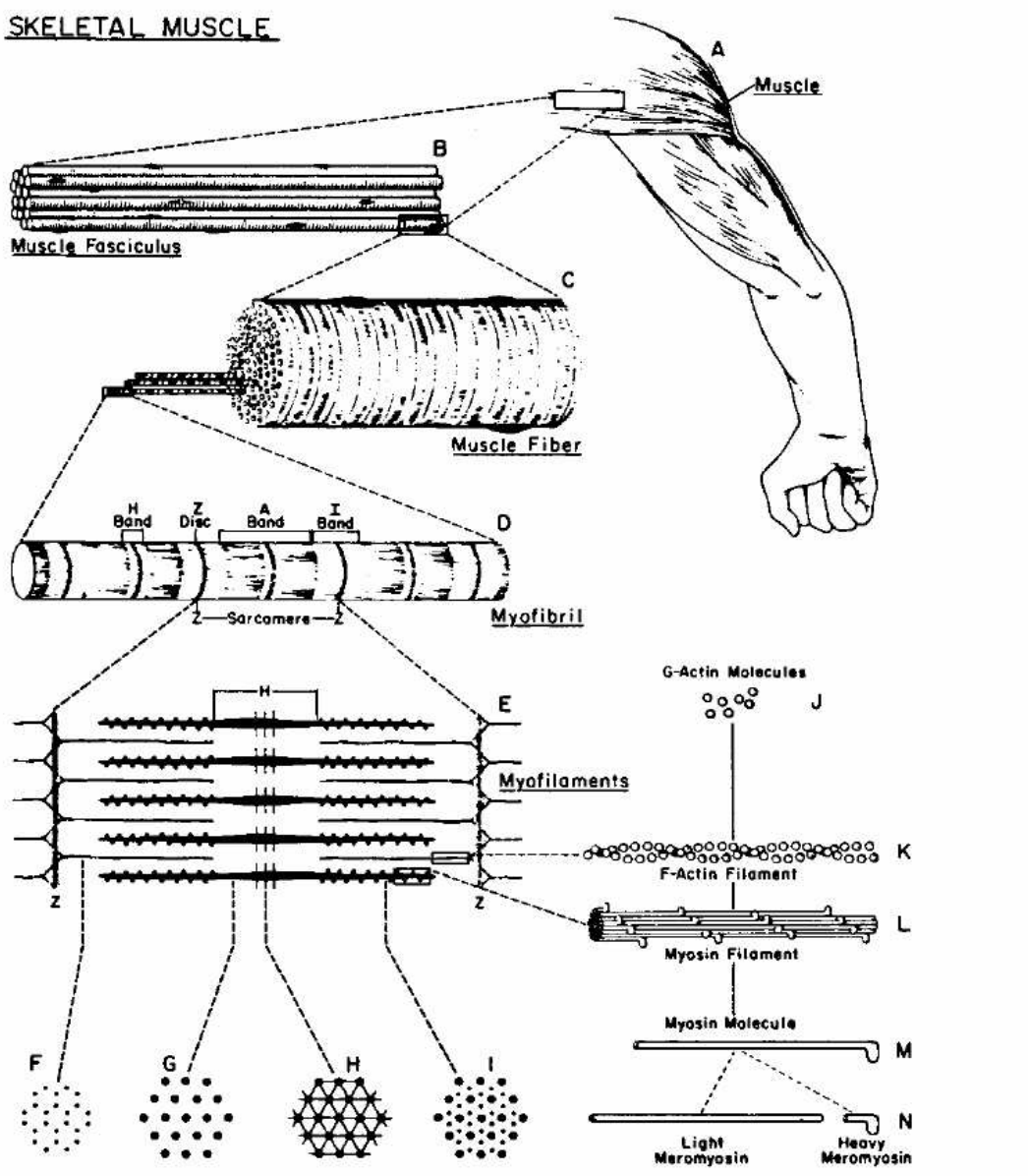

Figure 3-1 Organization of skeletal muscle [2].

part of the tendon which attaches the muscle and the bone as in Figure 3-2. The muscles are able to exert tensile forces due to this attachment. Second, the connective tissues help to bind contractile units and groups of units together so that their action is integrated. This arrangement allows independent functioning of the fibers. The independent

functioning of the fibers is important because the fibers belonging to the same motor unit can be spread throughout the muscle. Motor units are the smallest functional unit of the neuromuscular system. Contraction of single muscle fibers within many different fasciculi is the result of activation of a motor unit [2].

A muscle cell is surrounded by sarcolemma. The myofibrils that make up the muscle fiber are contained within the sarcolemma [Figure 3-1d]. The myofibril runs along the entire length of the muscle fiber [2].

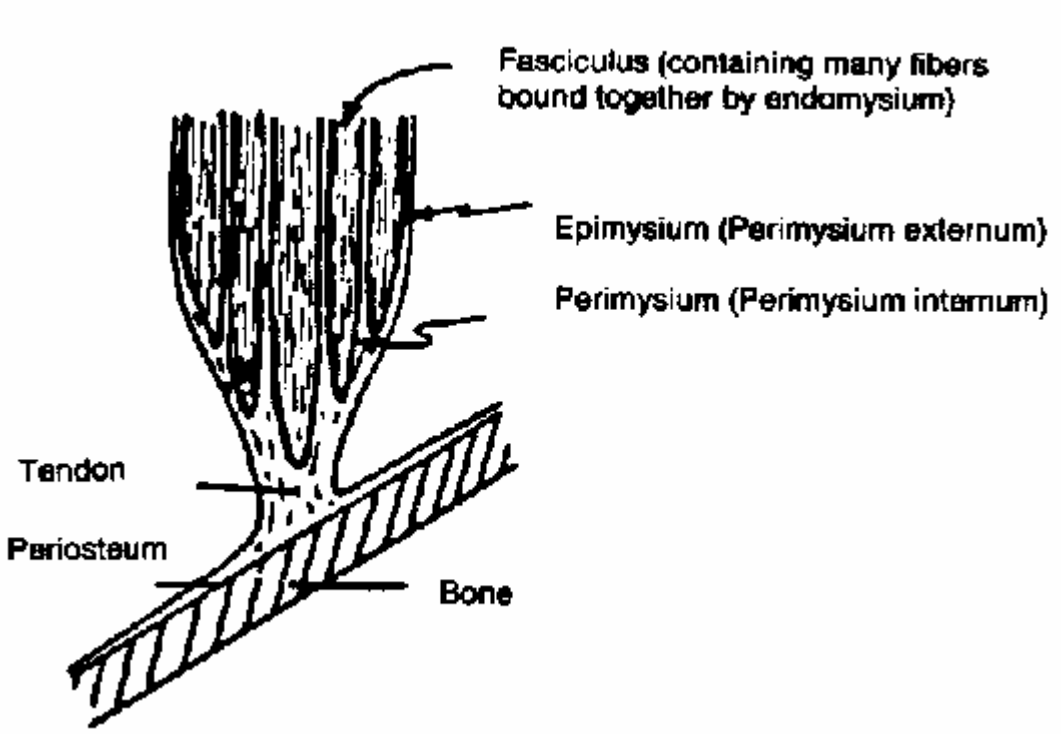

Figure 3-2 Cross structure of a skeletal muscle [2].

The sarcomere is the smallest contractile unit of the muscle. A series of sarcomeres form the myofibril. The total muscle fiber contraction is the end product of contraction of all the sarcomeres within [2].

3.2 The Electromyography Signal

The sarcolemma is a thin semi-permeable membrane composed of a lipid bi-layer that has channels through which certain ions can move between the intra-cellular and the extra-cellular fluid. The intra-cellular fluid has a high concentration of potassium (K+) ions and an organic (A-) anion. The K+ ions are small enough to pass through the channels in the membrane as opposed to the organic anions that cannot flow through the membrane. The extra-cellular fluid has sodium (Na+) and chloride (Cl-) ions. The Cl- ions are small enough to pass through the membrane channel, but the larger Na+ ions have difficulty in penetration (refer Figure 3-3) [2].

Let us consider for a moment that there is no difference in potential between the intra cellular and extra-cellular fluid (Figure 3-3). The K+ diffuses through the cell membrane because of higher concentration inside the cell compared with outside the cell. The Na+ ions cannot move in the opposite direction through the membrane to replace the K+ ions. Therefore, a potential difference develops across the sarcolemma membrane. A positive charge now develops on the outside of the membrane and this slows the further diffusion of K+ ions. The Cl- ions act in a similar manner and remain in equilibrium because of this interaction between its concentration gradient and the electrical charge [2].

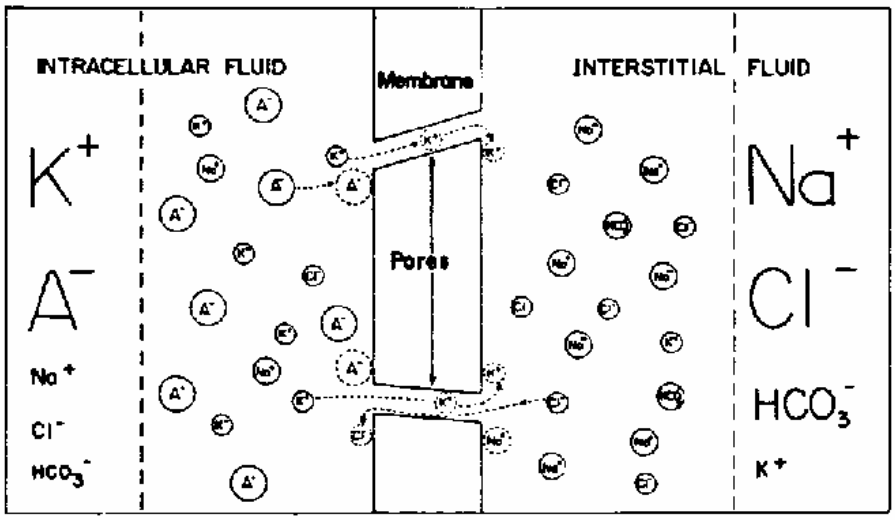

Figure 3-3 Development of trans-membrane voltage by an ion concentration gradient. Diagram of an intracellular fluid-membrane-interstitial fluid system. Membrane has some properties of a real cell membrane. The pores in the membrane are such that K+ and Cl- ions can pass through easily, Na+ with difficulty and A- ions cannot pass through [2].

The movement of K+ and Cl- ions creates a positive charge on the outside, and a negative charge on the inside of the membrane. Like charges repel each other and therefore, the positive charge on the outside of the membrane in combination with the large concentration gradient of Na+ drives Na+ into the cell. An active ion transport system called the sodium-potassium pump maintains the membrane potential [2]. This pump redirects the Na+ ions to the outside of the cell.

A muscle fiber contraction is preceded by several events. A depolarization is initiated in the motor neuron (muscles are stimulated by motor neurons) by the central nervous system. This depolarization is conveyed to the motor end plate through the motoneuron. At the endplate, a chemical substance is released that diffuses across the synaptic cleft causing a rapid depolarization of the muscle fiber under the motor endplate. This rapid depolarization, and the subsequent re-polarization of the muscle fiber, is an

action potential [2]. The action potential propagates along the muscle fiber in both directions, away from the motor end plate.

The basis of surface electromyography is the relationship between the action potential of muscle fibers and the extra-cellular recording of those action potentials at the skin surface. The motor unit consists of the motor neuron and the muscle fibers that it stimulates [19]. Few motor units are required to be activated for weak contractions. Stronger contractions require larger number of motor units to be activated or recruited to contract, and this selective activation of motor units is called motor unit recruitment [19]. The frequency of the stimulation of the motor units is called the motor unit firing rate.

3.3 Model for the Surface EMG Signal

The EMG signal may be modeled by linearly summing up the motor unit action potentials trains (MUAPTs) as they exist when they are detected by the electrode. This approach may be expressed as $m(t,F) = \sum_{i=1}^{p} u_i(t,F)$

Where $m(t,F)$ is the observed EMG signal being a function of time variable t and force F, $u_i(t,F)$ is the i^{th} motor unit action potential train (MUAPT) and p the total number of MUAPTs. A schematic representation of the model is shown in Figure 3-4. The integer p represents the total number of MUAPTs which contribute to the potential field at the recording site. The superposition at the recording site forms the physiological EMG signal, $m_p(t,F)$. However, the detected signal is affected by electrical noise n(t), and the filtering of the recording electrode r(t) [r(t) is the impulse response of the recording electrode]. The resulting signal, $m(t,F)$, is the observable EMG signal [6]. The location

of the recording site with respect to the active motor units determines the waveform of h(t) which is the motor unit action potential.

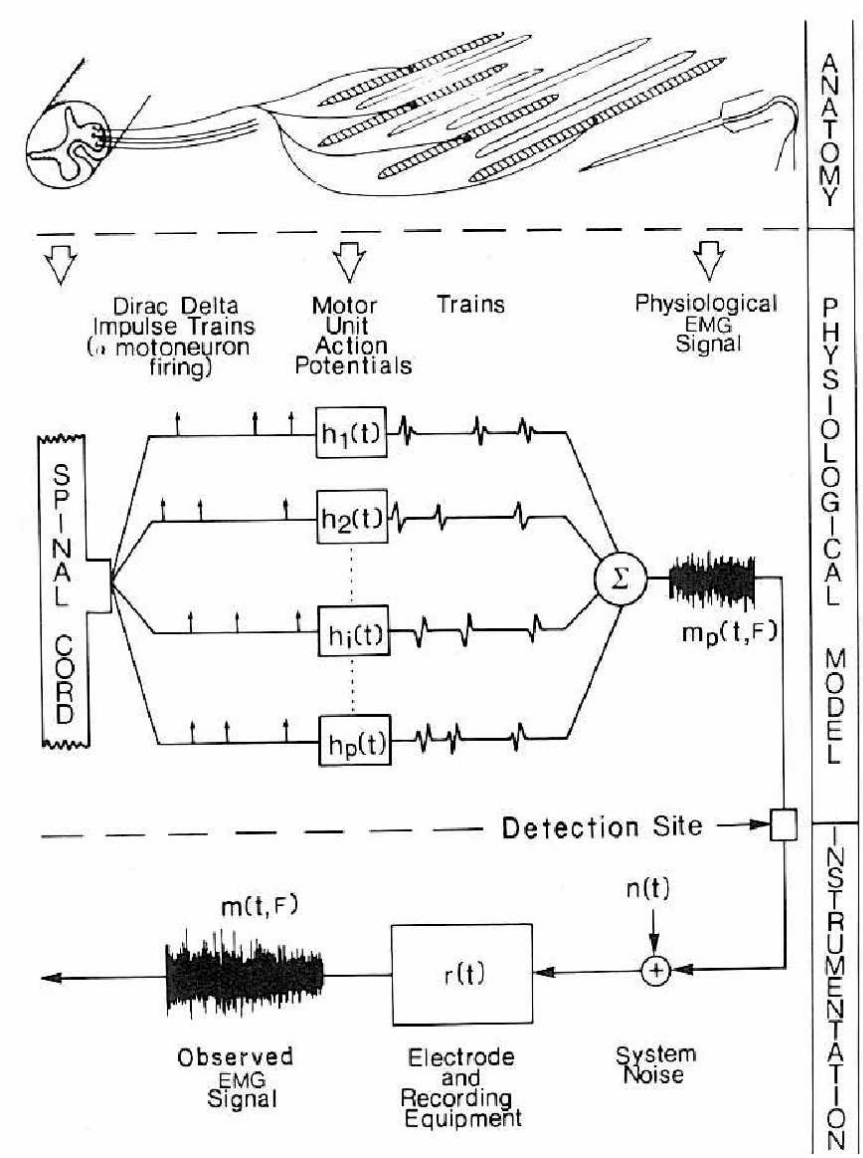

Figure 3-4. Schematic representation of the model for the generation of the EMG signal [6].

The MUAPT may be completely described by its inter pulse interval (IPI) and the waveform of the motor unit action potential (MUAP). It is convenient to describe the

MUAPT as a random process in which the waveform of the MUAP is present at random intervals of time. The MUAPT's can be divided into a sequence of dirac delta impulses $\delta_i(t)$, which are passed through a filter whose impulse response is $h_i(t)$. The impulse response of the filter can be modeled as time variant to reflect changes in the waveform of the MUAP during a sustained contraction.

If each dirac delta impulse marks the time occurrence of a MUAP in a MUAPT, the output of the filter will be the MUAPT or $u_i(t)$. The integer i denotes a particular MUAPT.

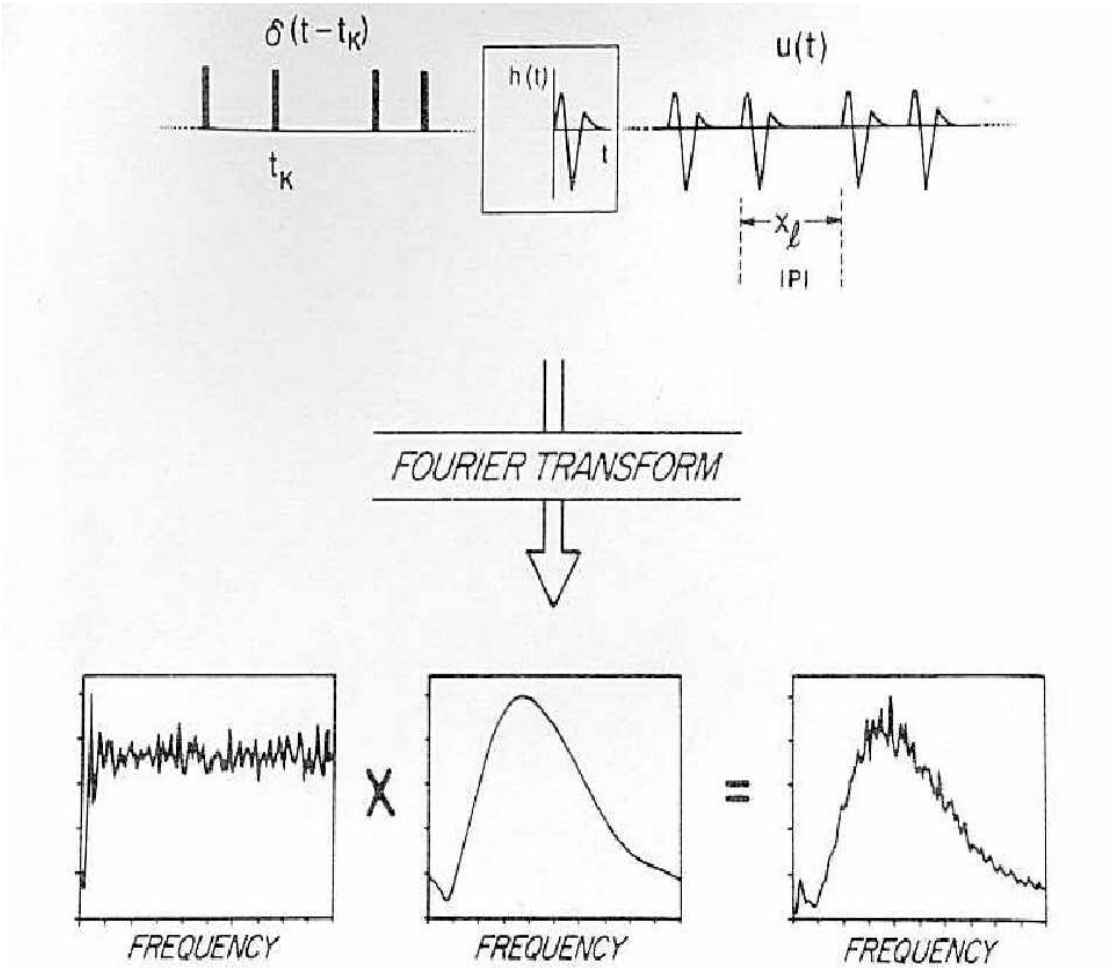

Figure 3-5 Model for a motor nit action potential train and the corresponding Fourier Transform of the inter pulse intervals (IPI), the motor unit action potentials and the MUAPT.

The dirac delta impulse train can be described by

$\delta i(t) = \sum_{k=1}^{n} \delta(t - t_k)$. Therefore the MUAPT $u_i(t)$ can be formulated as

$u_i(t) = \sum_{k=1}^{n} h_i(t - t_k)$,where $t_k = \sum_{l=1}^{k} x_l$ for k,l=1,2,3,…n.

The variable t is a real continuous random variable, t_k represents the time locations of the MUAPs, x represents the IPIs, n the total number of IPI's in a MUAPT, and i, k and l are the integers which denote specific events [6].

3.4 Relating Electromyogram to Torque

Researchers have been studying the relationship between the surface electromyogram and the torque produced about a joint, to estimate musculoskeletal load in particular and joint dynamics in general. Measurement and understanding of these dynamics is important in the prevention of musculoskeletal injuries in the workplace and in rehabilitation engineering, basic motor control research and neuromuscular diseases.

There has been experimental study by Clancy and Hogan relating simultaneous elbow flexor and extensor electromyogram amplitude to joint torque [3]. There are a few assumptions made while forming this relationship. First, that the EMG amplitude can be identified from the EMG waveform. Second, for the case of isotonic, isometric and non-fatiguing muscle contractions, the EMG amplitude has a constant value. Third, that the joint torque is an identifiable function of EMG amplitude. Torque measured about a joint is assumed to be algebraically related to the torques due to flexion (T_F) and extension (T_E) as $T_{EXT} = T_F - T_E$. The flexion and extension EMG amplitudes are in turn related to the flexion and extension torques as the polynomials:

$$T_F = f_{F,1} \bullet s_F + f_{F,2} \bullet s_F^{\,2} + f_{F,3} \bullet s_F^{\,3} + \ldots$$

Equation 3-1

$$T_E = f_{E,1} \bullet s_E + f_{E,2} \bullet s_E^{\,2} + f_{E,3} \bullet s_E^{\,3} + \ldots$$

Equation 3-2

$$T_{EXT} = T_F - T_E$$

Equation 3-3

where $f_{i,j}$ are the fit parameters, s_E is the EMG extension amplitude estimate and s_F is the flexion amplitude estimate. The error between the estimated and measured torque at each instant in time (t) was $error_t = T_{Ft} - T_{Et} - T_{extt}$. For a sequence of measurements, linear least squares techniques were used to calculate the fit parameters to minimize the mean squared error between the measured and estimated torque [3].

3.5 Joint Dynamics

The dynamic relation between joint position and torque is referred to as joint dynamics. Linear models provide good descriptions of joint dynamics provided that conditions (eg: activation level, mean position) are maintained approximately constant over the experiment [5]. Parametric or non-parametric models can be used for describing the system behavior. Parametric models describe system behavior in terms of an analytic expression. Systems may be described with relatively few parameters, if the correct model order is chosen. Non parametric models use descriptions such as impulse response functions or frequency response functions that make no assumptions about model order or system structure and are infinite dimensional in nature.

Researchers such as Kearney and Hunter have studied the human ankle joint dynamics by applying stochastic perturbations of position [7]. Their experiments consisted of nominally constant posture, constant force and non-fatiguing contractions. The subjects were trained to maintain a steady contraction in either plantar flexion or dorsiflexion during ongoing perturbations. Subjects were asked to maintain a constant effort whose magnitude was adjusted with respect to the visual feedback of the torque. Prior to each experiment, subjects were informed about the required level of contraction. To avoid muscle fatigue, contractions were limited to less than 20% maximum voluntary contraction (MVC). The mean EMG level was always monitored and if there was an increase in EMG activity (implying muscle fatigue) then subsequent trials involving higher mean torque were not performed. The idea was to understand the system under normal conditions and not when it is under fatigue. The ankle position and torque were low-pass filtered (8 pole Bessel, 200 Hz cut-off) to avoid aliasing and then sampled at 400 Hz by a 12 bit A/D converter for 65 seconds [7].

Figure 3-6 shows the time domain ankle torque and position measurements collected during one such experiment.

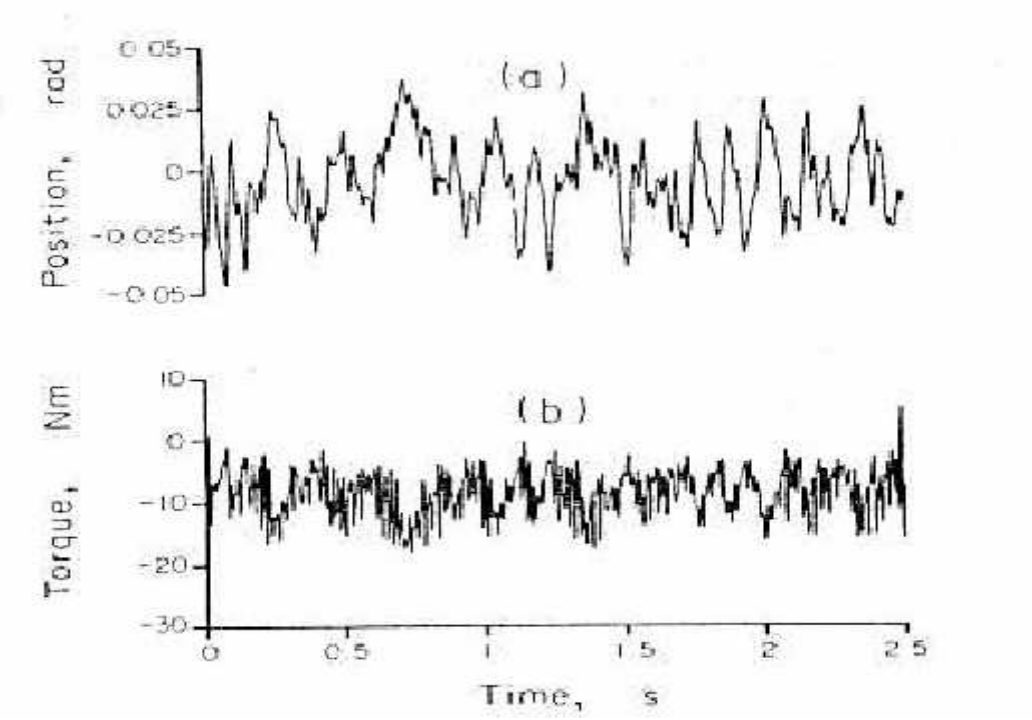

Figure 3-6 Measured values of (a) angular position and (b) torque of the ankle [7]

Position data are considered to be the input to the system and the joint torque as the output. The transfer function of the system is the system output divided by the input in the frequency domain. Thus, frequency analysis techniques consist of taking the Fourier transform of the measured torque deviations and displacements and dividing one by the other. The result is the transfer function of the joint.

Frequency analysis techniques were employed on the data to obtain the ankle impedance gain and phase (nonparametric technique) after removing the bias (subtracting the mean value) from the torque and position measurements. Figure 3-7 shows the gain and phase characteristics of the impedance using the measurements obtained. The curves obtained were compared with the characteristics of a second order system [smooth line in

Figure 3-7 (a) and (b)]. It can be observed that the two curves are close to each other suggesting that a second order system can be a good approximation to model joint dynamics.

Coherence is defined as

$$|\gamma_{T,\theta}(j\omega)|^2 = \frac{|\phi_{T,\theta}(j\omega)|^2}{\phi_{T,T}(j\omega)\phi_{\theta\theta}(j\omega)}$$

Equation 3-4

where $\phi_{\theta\theta}(j\omega)$ is the position auto spectrum, $\phi_{T,\theta}(j\omega)$ is the torque-position cross-spectrum and $\phi_{T,T}(j\omega)$ is the torque auto-spectrum. The coherence squared (frequency domain characteristic of output variance accounted for) gives us an estimate of how much of the output power can be predicted on the basis of the linear transfer function estimate at each frequency [5]. Figure 3-7 (c) shows that we have a high value of coherence (0.9) for most of the frequency range, suggesting that this estimate of the transfer function is a good approximation [7].

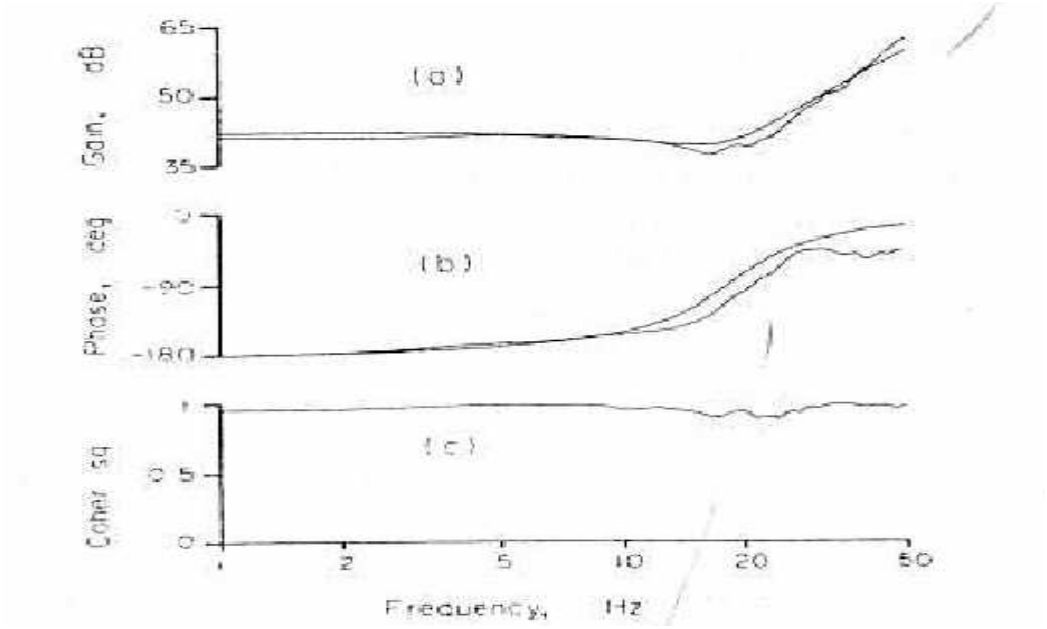

Figure 3-7 Frequency analysis of the data shown in fig 2-5. (a)Stiffness gain in dB,(b) phase in degrees (c) Coherence squared. Smooth curves are plots for a second order system, jagged curves for the actual data [7].

From the above analysis, the system seems very similar to a second-order system. The transfer function can be therefore be modeled as

$$STIFF(s) = \frac{TQ(s)}{POS(s)} = Is^2 + Bs + K$$

Equation 3-5

where:

STIFF= dynamic ankle impedance, TQ = torque deviations, POS = angular deviations, I is angular moment of inertia (of the foot) in Nms^2/rad, B = angular viscosity in Nm-s/rad, K=angular elasticity of the ankle in Nm/rad and $s = jw$ is the complex frequency.

Therefore, joint dynamics (under constant operating point conditions) have frequently been modeled using a parametric model of the form

$$\Delta T(t) \quad = \quad I\frac{\partial^2 \Delta\theta(t)}{\partial t^2} \quad + \quad B\frac{\partial \Delta\theta(t)}{\partial t} \quad + \quad K\Delta\theta(t)$$

Equation 3-6

where, $\Delta T(t)$ = change in torque, $\Delta\theta(t)$ = change in angular position, I = inertial parameter, B = viscous parameter, K = elastic parameter [5]. An advantage of using Equation 3-6 to model joint dynamics is that each parameter has a direct interpretation in terms of the underlying physics [5]. Equation 3-6 is the time domain equivalent of Equation 3-5 assuming zero initial conditions.

Kearney and Hunter [7] performed a time domain parametric analysis to find out the best fit parameters (K, B and I). These parameters were plotted for various bias torque values. These estimated parameters varied with mean ankle bias torque. The elastic (K) and viscous (B) parameters increased linearly with increase in bias torque (over their range of bias torques) but the inertial (I) parameter did not change much with torque [7].

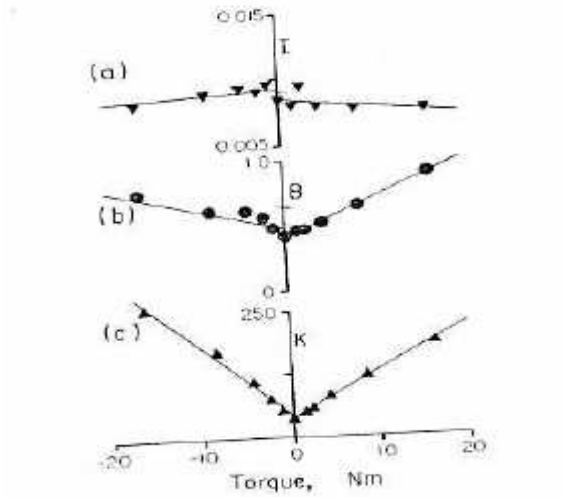

Figure 3-8 (a) Inertial(Nm s^2/rad), (b) viscous (Nm s/rad) and (c) elastic parameters(Nm/rad) estimated in the time domain as functions of mean ankle torque. Positive and negative torques corresponds to dorsiflexing and plantar flexing[7].

The operating point is defined by the mean torque or mean position (maintained by the subject via feedback). The operating point remains constant over a particular trial consisting of constant posture, constant force, and non-fatiguing contractions. The parameters change as the operating point changes. The ensemble of linear models estimated over a range of operating conditions may be thought of as defining a quasi-static model of joint dynamics and can be defined by the linear equation

$$\Delta T(t) = I\frac{\partial^2 \Delta\theta(t)}{\partial t^2} + B(\lambda)\frac{\partial \Delta\theta(t)}{\partial t} + K(\lambda)\Delta\theta(t)$$

Equation 3-7

where λ defines the operating point of the system. The quasi-static model cannot be used when the operating point of the system is changing dynamically [5].

3.5.1 Impedance measurement using EMG

Osu and Kamimura [8] have performed experiments collecting surface EMG activity from the brachioradialis, medial head of the triceps brachii (mono-articular muscles), biceps brachii and long head of the triceps (bi-articular muscles). The EMG signals were high pass filtered at 25Hz, low-pass at 1 KHz and sampled at 2KHz. The digitized EMG signals were rectified and averaged for a period of 0.4 seconds before perturbations. Using previous studies by Osu and Gomi [9] which had suggested a linear relation between surface EMG activity and joint torque and joint stiffness, a parameter called index of muscle co-contraction around the joint (IMCJ) was introduced.

First, joint torque was expressed as the difference between the flexion torque exerted by the flexor muscles and the extension torque exerted by the extensor muscles [10].

Elbow torque can be expressed as $\tau = a_1 s_{F1} - a_2 s_{E1} + a_3 s_{F2} - a_4 s_{E2}$

Equation 3-8

where s_{F1} and s_{E1} are the surface EMG activity of the elbow mono-articular flexor and extensor, respectively and s_{F2} and s_{E2} denote surface EMG activity of bi-articular flexor and extensor, respectively. The EMG activity (s_E, s_F) and torque are measured. The parameters a_i include both the moment arm and the conversion factor from muscle activity (rectified and averaged EMG) [10] to muscle tension. The a_i terms are constants for a constant moment arm (i.e. limb posture).

If each muscle stiffness term is proportional to the corresponding muscle torque ($a_i s_{Ei}$), we can use summation of muscle torque as an indicator of joint stiffness [10]. Stiffness can be related to the weighted summation of rectified EMG signals through the index of muscle co-contraction around the joint (IMCJ) [8]. IMCJ can be defined as the summation of absolute values of antagonist muscle torques around the joint, and it is computed from the linear relation between surface EMG and joint torque.

$$IMCJ = a_1 s_{F1} + a_2 s_{E1} + a_3 s_{F2} + a_4 s_{E2}$$

Equation 3-9

From Equation 3-8 and Equation 3-9, concomitant increases in flexor and extensor muscle torques do not increase joint torque but do increase the IMCJ because IMCJ is the summation of absolute values of muscle torques [*10*].

To check the utility of IMCJ, the IMCJ estimated from EMG was compared to the stiffness measured using conventional methods of applying mechanical perturbations. Perturbations were applied by a manipulandum fixed to the subjects arm. The subjects arm was pushed and pulled back in eight random directions (6-8 mm) in a short period of

time (0.3 seconds). The subjects were asked to keep the muscle (EMG) activity constant during the trial. A second order model was used to estimate the stiffness (Nm/rad) [10]. The EMG was recorded (using silver electrodes) from the elbow muscles and signal processing techniques discussed above (rectification and averaging) were applied. The processed EMG was used as the muscle activity u_i in Equation 3-8. The force was measured using a force sensor attached and averaged over a period of 0.4s.The joint torque was calculated from the average force. It was confirmed that IMCJ linearly correlated with the stiffness measured directly by applying mechanical perturbations to the arm during isometric force regulation tasks.

IMCJ is not a universal indicator for stiffness since there can be variable moment arms during movements and non linear properties of muscle tension. IMCJ does not estimate viscosity and inertia. However, IMCJ is useful under certain limiting conditions where the second order system contributions of viscosity and inertia are limited. The above method would not benefit from using advanced EMG amplitude estimators due to the usage of a long (0.4sec) averaging window. The simple linear model of Equation 3-9 does not capture all subtleties of the stiffness parameter, but definitely is a good first approximation of stiffness to be measured from EMG activity [8].

4 Simulation Methods and Results

Simulations were first performed in MATLAB before the processing methods (discussed later in the section) were applied to experimental data. All our simulations had the change in angular deviation ($\Delta\theta$) as the input to the system and change in torque (ΔT) as the generated output. Simulations helped address some of the concerns in processing the data. First and second derivatives of angular measurements had to be taken which could introduce high frequency noise. The low-pass filters required to deal with this high frequency noise had to be designed. Torque measurements in an experimental set up usually have a low frequency artifact component associated with it. This low frequency component arises due to the fact that the subject is expected to maintain a constant background force level during a trial. In an attempt to maintain this background force level, the subject could drift about from the expected background force, and this drift manifests itself as a low frequency artifact. This artifact is called the bias torque. This slowly varying torque bias has to be removed from the measurements before system identification is performed. Methods such as high-pass filters and subtraction of a polynomial were implemented to rid this low frequency component. A new model (explained in section 4.5) relating EMG amplitude to impedance was devised as an extension of the change in torque to change in angle relationship (explained in section 3.5). This new approach of estimating impedance using EMG was simulated to find out what duration data need be collected and to understand the effect of noise (in EMG amplitude estimates) on estimation of impedance parameters.

The second order linear equation relating angular position to the change in torque produced about the joint is given by:

$$\Delta T = K\,\Delta\theta + B\,\Delta\dot{\theta} + I\,\Delta\ddot{\theta}$$

Equation 4-1

where
K is the elastic parameter,

B is the viscous parameter,

I is the inertial parameter,

$\Delta\theta$ is the change in angular displacement of the joint and

ΔT is the change in torque produced about the joint.

4.1 Parameters and Basic Procedures

4.1.1 Sampling Rate and Duration

A sampling frequency of 256 Hz was used and the simulated recording time was 30 seconds per trial.

4.1.2 Stimulus

The angular deviation $\Delta\theta$ was the stimulus for our system. The angular deviation signal was simulated using a pseudo-random binary sequence (PRBS) generator (varying between 1 radian and -1 radian) followed by a low-pass Butterworth filter with a gain of 1 in the pass band and a cut-off frequency of 3 Hz. The peak-to-peak displacement amplitude was clipped to 0.05 radians (2.86 degrees). Earlier experiments by Kearney and Hunter [4, fig 1] indicate perturbations of 0.05 radians as sufficient for producing

torque variations of about 12 N-m.

4.1.3 Theta Quantization

Quantization noise in θ arises due to the fact that we use an encoder to encode the angular deviations in the experimental apparatus. The encoder uses 48,000 counts per 360 degrees. The generated θ in our simulation model is therefore quantized to mimic the encoder. There could additionally be some random noise in the form of measured noise (in the encoder) which is not greater than one count in the encoder. The effect of this random noise is very minimal due to the accuracy of the encoder. Therefore only the quantization error was considered.

4.1.4 Derivatives

A central differences followed by a low-pass filter scheme was used to take the first and second derivatives of $\Delta\theta$.

$$y[n] = \frac{x[n+1] - x[n-1]}{2 * \Delta t}$$

Equation 4-2

where $x[n]$ is the input,
$y[n]$ is the derivative and
Δt is the sampling time.

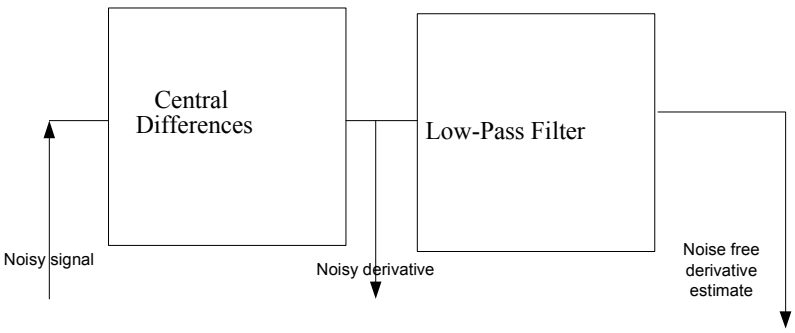

Figure 4-1 Basic differentiator estimate

The derivatives were followed by low-pass filters to filter away the noise due to the first stage. The low-pass FIR filter, the cut-off frequency and the number of taps to be used was determined by simulation for the first and second derivatives (described below).

4.1.5 Parameter Estimation

Impedance parameter estimation consists of estimating K, B and I (in Equation 4-1) given ΔT and $\Delta\theta$ using the above model equation. ΔT and $\Delta\theta$ are the measured values. The first and second derivatives, $\dot{\theta}$ and $\ddot{\theta}$ are calculated from θ. $\hat{K}, \hat{B}$ and $\hat{I}$ are then found using the method of linear least squares. For the simulation, we start with known values of K, B, I (using [13]) and θ. $\hat{K}, \hat{B}$ and $\hat{I}$ are then calculated using ΔT and $\Delta\theta$. The estimated and known values are compared.

The model equation in Equation 4-1 suggests that, given the torque deviations (ΔT) and measured angular deviations ($\Delta\theta$), we can numerically evaluate $\Delta\dot{\theta}$ and $\Delta\ddot{\theta}$. Therefore, the unknown quantities are then K, B and I. The general form of this kind of model is

$$y(x) = \sum_{k=1}^{M} a_K X_k(x)$$

Equation 4-3

where $X_1(x), X_2(x),...X_M(x)$ are arbitrary functions of x called basis functions [12]. The basis functions can be non-linear by themselves but the model's dependence on the system parameters a_k is linear. In our model, $X_1(x) = \theta, X_2(x) = \dot{\theta}, X_3(x) = \ddot{\theta}$ and $a_1 = K, a_2 = B \text{ and } a_3 = I$.

For our model, we define a merit function as

$$\chi^2 = \sum_{i=1}^{N} \left[y_i - \sum_{k=1}^{M} a_k X_k(x_i) \right]^2$$

Equation 4-4

The linear least squares problem is to minimize χ^2 and to pick the a_k values that achieve the least χ^2. Let A be a matrix having M columns each representing the M basis vectors ($\theta, \dot{\theta}, \ddot{\theta}$ for our case) and N rows representing the function evaluated (or measured) at N data points. Therefore, we have $A_{ij} = X_j(x_i)$. The matrix A is the design matrix of the fitting problem. Also, we define a vector **b** of length N as b = $[y_1, y_2, ...y_N]^T$ and vector **a** whose components are the parameters to be determined. $[a_1, a_2, ..., a_M]^T$. For our case, $A = [\theta\ \dot{\theta}\ \ddot{\theta}]$ $\theta\ \dot{\theta}\ \ddot{\theta}$ are column vectors of length N, $b = \Delta T$ the measured torque of length N and a= [K B I].

The minimum of Equation 4-4 occurs when the derivative of χ^2 with respect to all M a_k parameters goes to zero. To solve the linear least squares problem, the normal equations in matrix form are [12]:

$$(A^T \bullet A)a = A^T b$$

4.2 Simulation for Derivative Filters

As explained in 4.1.3, the encoder that is used for recording the angular deviations introduces high frequency quantization errors. High frequency components exist at the output of the quantizer, since the quantization process inherently introduces steps (high frequency content) and also due to truncation errors in the encoder. Our model equation (Equation 4-1) requires that we take first and second derivatives of the angular deviations. An ideal differentiator has a frequency response magnitude of $|H(\omega)| = \omega$ which is a linear function of frequency. The presence of high-frequency noise in the signal would result in very noisy derivatives, since the ideal differentiator would provide a higher gain to the high frequency noise as opposed to the low frequency signal. This operation of the differentiator could result in noise being the major component of the derivative estimate. Therefore, we find the necessity to design and implement low-pass filters to remove this noise to obtain better derivative estimates. The objective of the present simulation was to examine various filters to reduce the effect of noise at the output of a differentiator and achieve better derivative estimates in the process.

The numerical central differences (Equation 4-2) approach is clearly a non-causal operation since the output depends on future inputs. Hence this approach can be used for applications where the future inputs are available, as they are in our case. Figure 4-2 shows a plot of the magnitude response of the ideal differentiator and the central differences system (approach used). We observe that the response of the central differences approach is very close to the ideal differentiator until around $\pi/6$ radians (on

a relative frequency axis) and then falls off from the ideal response. If our discrete time signal is sampled at a sufficient rate (much higher than the Nyquist rate), noise until around $\pi/6$ radians would be amplified (for example, if the signal is present until $\pi/12$ radians and the rest is noise).

Figure 4-3 shows the flow of the simulations performed. A signal (resembling an ideal angular position signal) is generated, which is then quantized to simulate the encoder. Numerical first derivatives (or second-derivatives as the case may be) of the un-quantized signal and the quantized signal (actual derivative) are taken. The numerical derivative of the un-quantized signal is treated as the "true" derivative. MATLAB uses double precision floating point and therefore the central differences of the double precision floating point is used as the true derivative. The quantized signal, after the central differences, is passed through various low-pass filters (estimated derivative) and then compared with the "true" derivatives. The filter providing the lowest RMS error (explained in section 4.3) will be used for the derivative filter.

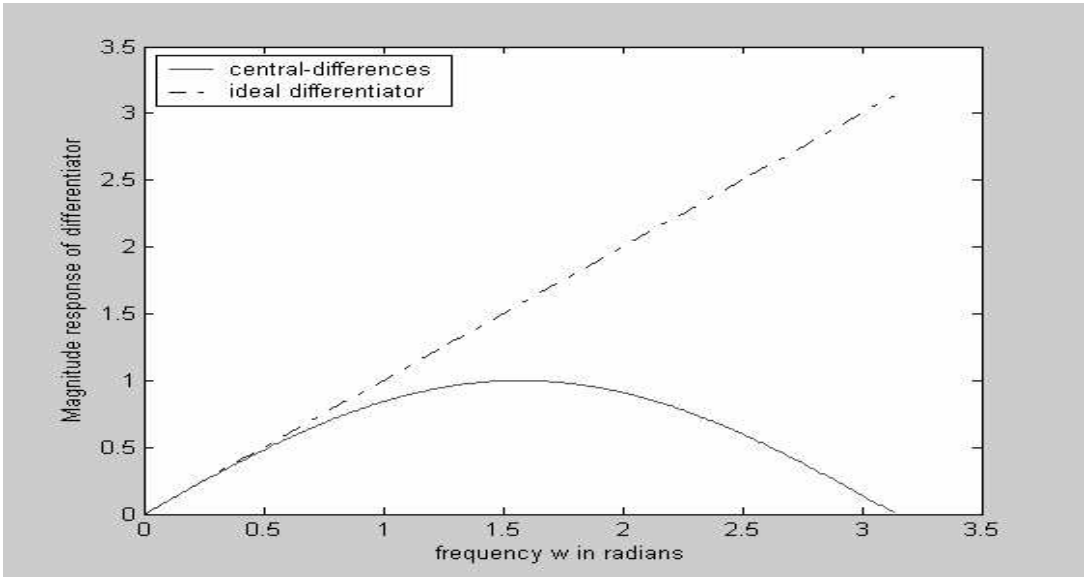

Figure 4-2 Magnitude response of ideal differentiator v/s that of numerical central differences approach.

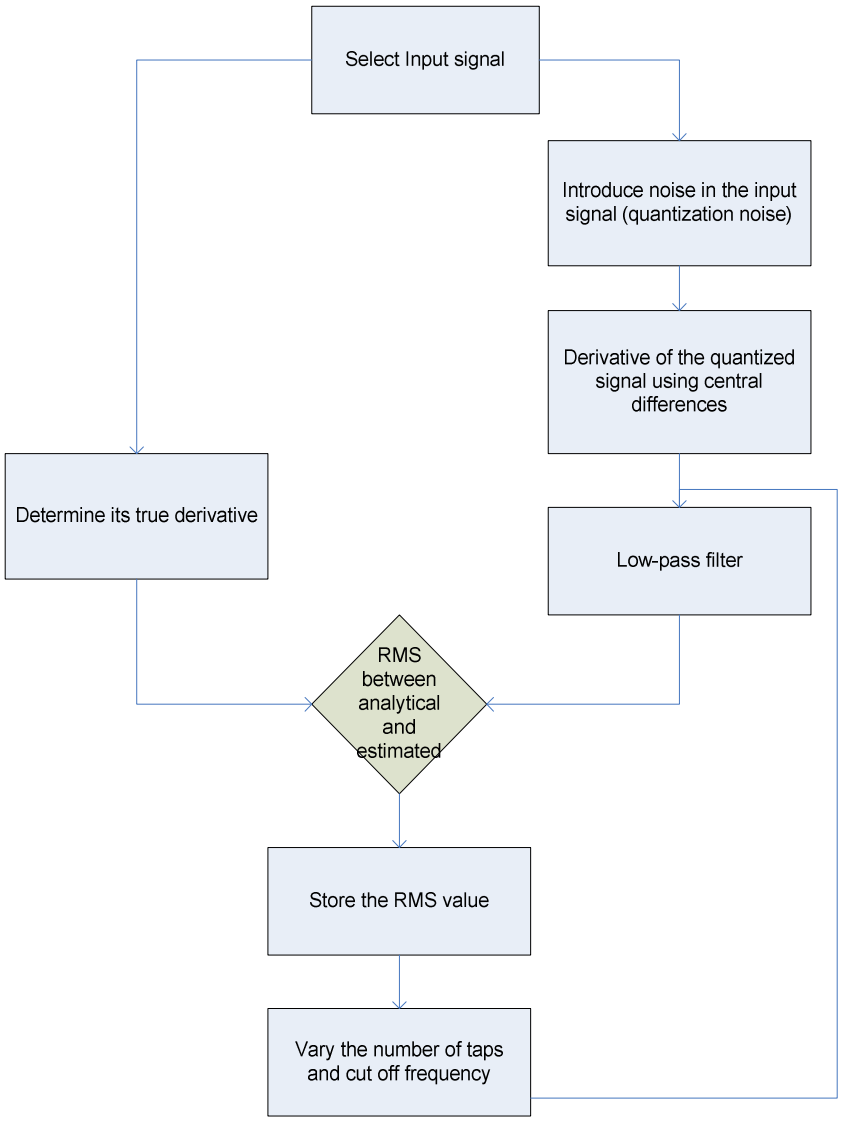

Figure 4-3 Basic block diagram of the simulation for derivative filters

4.2.1 Low Pass Filter

A Hamming window-based, finite impulse response (FIR) low-pass technique was used to design the low-pass (LP) filter [17]. However, the order and the cut-off frequency of the filter were varied to investigate the performance of the derivative estimate. Zero-phase filtering (Matlab's function filtfilt [18]) was performed to eliminate phase distortions within the low-pass filter. The start-up transients of the FIR filter were removed before making the error evaluation.

4.3 Simulations and Results for Derivative filters

The root-mean-square (RMS) difference was taken between the "true" derivative and the estimated derivative (signal after quantization and low pass filtering).

$$RMS\ error = \sqrt{\frac{\sum (x_{actual} - x_{estimate})^2}{N}}$$ N being the number of elements.

Figure 4-4 shows a plot of RMS error obtained in estimating the derivatives using the central differences followed by a low pass filter. The cut-off frequency has been varied from 4.26 Hz to 84.26Hz in steps of 10 Hz., and the number of taps of the low-pass filter have been varied from 10 to 300 in steps of 20. Each curve in the plot represents the filter at a particular cut-off frequency. The RMS error is quite similar for cut-off frequencies of 64 Hz and higher. Also, there is no appreciable change in the RMS error with increase in the number of taps at these higher cut-off frequencies. However, the best low pass filter to be used will be the one with the least RMS error on this plot (Figure 4-4). The RMS error is least with a filter of length 10 and a cut off frequency of 84.2667 Hz.

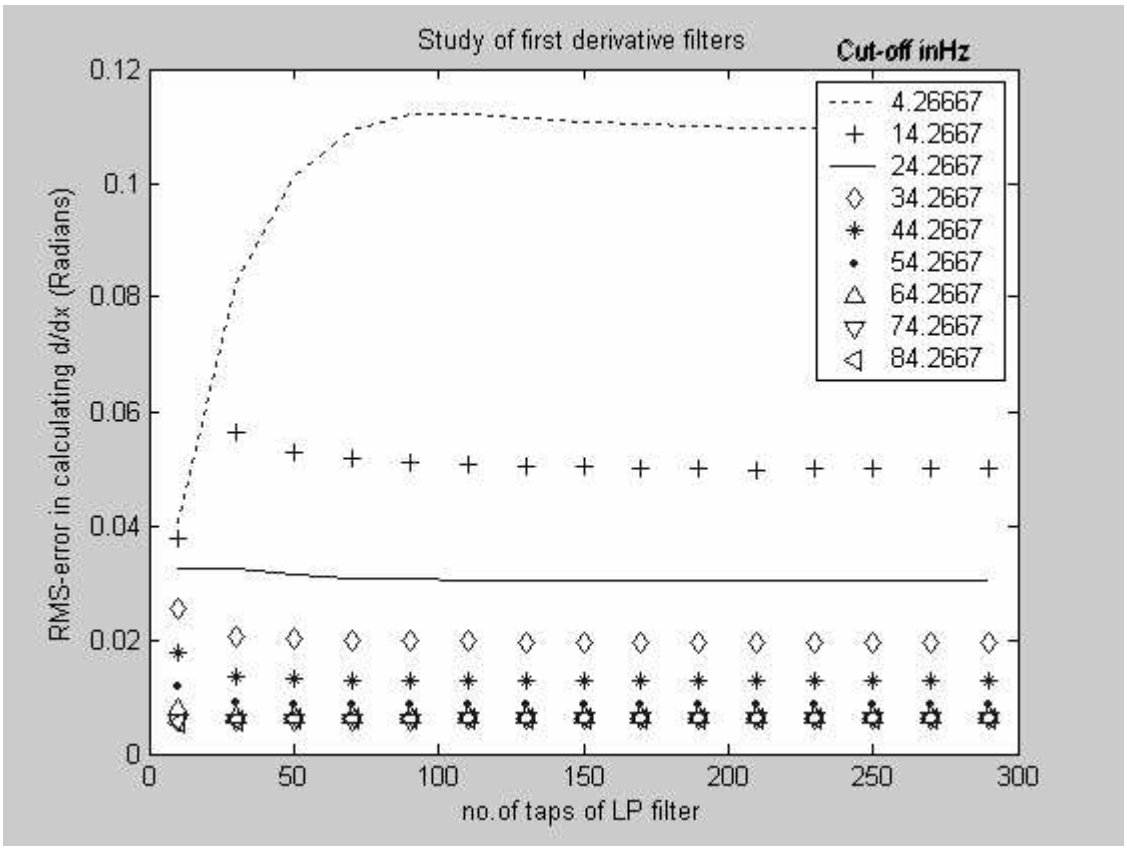

Figure 4-4 RMS error obtained for the first derivative estimates, each curve represents different cut-off frequencies.

Figure 4-5 shows a plot of RMS error values when low pass FIR filters of various cut-offs are used, while estimating the second derivatives. The cut-off frequency has been varied from 4.26 Hz to 84.26Hz in steps of 10 Hz., and the number of taps of the low-pass filter have been varied from 10 to 300 in steps of 20. The RMS error is quite similar for cut-off frequencies of 64.26 Hz and higher. Also, there is no appreciable change in the RMS error with increase in the number of taps at cut-off frequencies of 64, 74 and 84 Hz. However, the RMS error is least with a filter of cutoff 84.26Hz and 10 taps.

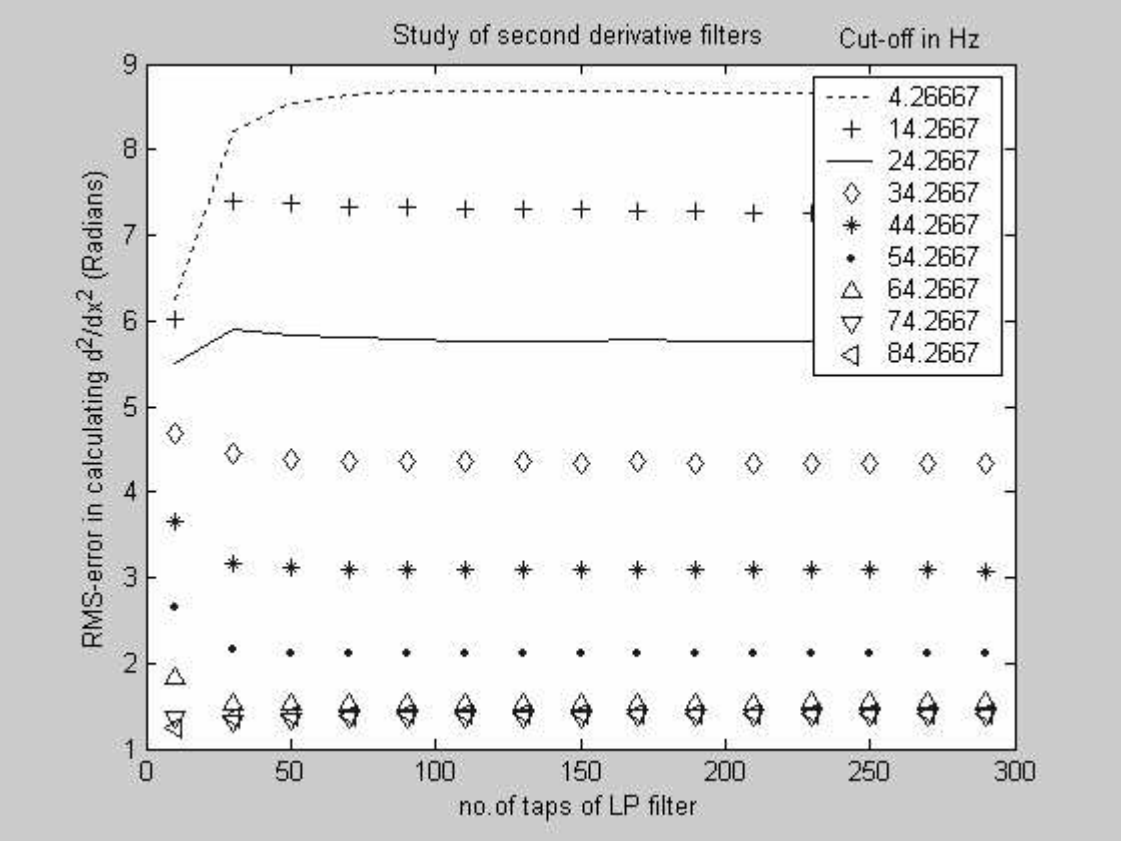

Figure 4-5 RMS error obtained for the second derivative estimate, each curve represents different cut-off frequencies.

The above simulations have provided a means to determine the type of filter to be used to remove the high frequency component (present due to the encoder) in the angle data. FIR filters with various taps and cut-off frequencies were used to determine the best filter to use. For the first derivative, an FIR filter of length 10 and cut-off frequency of 84.266 Hz is the optimal. The same filter of length 10 and cut-off of 84.26Hz is optimal for a second derivative.

4.4 Estimation of ΔT and $\Delta\theta$ for Varying Operating Point Contractions

Under the conditions of slowly varying background torque, the measured torque has a low frequency artifact component associated with it. This low frequency component arises due to the fact that the subject is expected to maintain a particular background torque level during a trial. In an attempt to maintain this background torque, the subject drifts about from the expected background force, and this drift manifests itself as a low frequency component. This low frequency component is not related to the perturbations themselves. For system identification, we need the ΔT signal and the position signal $\Delta\theta$. The measured torque is modeled as the background torque plus the ΔT:

$$Measured\ Torque = Background\ torque + \Delta T$$

Equation 4-5

Further, the background torque that the subject actually produces about the joint is different from the background torque that he/she is requested to produce. The background torque that the subject actually produces might be a slowly varying curve when he/she is expected to produce a straight line. This background torque has to be removed from the measured torque to get the ΔT. The ΔT is used for system identification as per our model equation in Equation 4-1, repeated here.

$$\Delta T = K\,\Delta\theta + B\,\Delta\dot{\theta} + I\,\Delta\ddot{\theta}.$$

There are a couple of approaches that were investigated for removing the background torque. Considering the background torque as a slowly varying component in comparison with ΔT, we used high-pass filters to remove the background torque. The high-pass filters were FIR and IIR. The FIR filters themselves were designed using a

window-based approach and least squares. Butterworth IIR filters were used for these simulations.. The slowly varying component was also removed by subtracting out the best fit polynomial from the total torque. For the purposes of simulation, we used values of K = 95 N-m/rad, B=2.9 N-m-s/rad and I=0.125N-m-s^2/rad corresponding to a torque bias of 40N-m for a time duration of 30 seconds [13].The methods were first applied to a constant operating point condition (constant torque bias) followed by a varying operating point (torque varying as a ramp). The ramp torque varied from 0 N-m to 30 N-m in a 30 second time period.

4.4.1 Window-Based FIR Filters

To find out the effects of high-pass filters on ΔT, we first passed the simulated ΔT signals (i.e. the torque signal with no background torque) through a high-pass filter and measured the amount of distortion caused to the required signal (ΔT). Various FIR filters were used. One of the common FIR filter algorithms is the window based approach. The errors in estimating the impedance parameters K, B and I were found in each case when ΔT was passed through various high pass filters of varying cut-off frequencies and taps.

The next task was to evaluate the effects of high pass filters on the total torque. The total torque was passed through various high pass filters in order to remove the slowly varying component of bias torque. The stiffness, viscosity and inertia were estimated after the total torque was passed through the filters. The errors in the actual parameters and their estimates were calculated for each filter operation. The difference in the actual impedance parameters and the estimated parameters was calculated as the error and taken as a percentage of the actual parameter.

The following plots show the percentage errors in estimation for each filter as a function of the high-pass cut-off frequency. Figure 4-6 shows a plot of the errors for the window based FIR filter approach of filter order 200 and varying cut-off frequencies. The errors for K and I are high for even low cut-off frequencies of up to 1Hz. Figure 4-6 shows that there is an error of about 50% in estimating the stiffness using the model when the total torque is passed through a FIR filter of order 200 and cut-off 1 Hz. The order of the filter was increased to 400 (Figure 4-7), 600 (Figure 4-8) and then 800 (Figure 4-9) for the same window-based FIR filter approach. The errors in estimating the parameters do not reduce considerably when the order of the filters is increased. With a filter order of 400 (Figure 4-7), the error in estimating K is 37% for a FIR filter with high pass cut off of 1 Hz which is still high. Therefore the window based FIR high pass filter is not an effective way to deal with the bias torque problem. Figure 4-9 shows that the error reduces moderately for higher order filters (of order 800). However, filters of order 800 have a start-up-transient of 800 samples which corresponds to about 3 seconds of data at a sampling rate of 256 Hz. The large amount of transients would mean losing out on too much data which could otherwise be used for system identification.

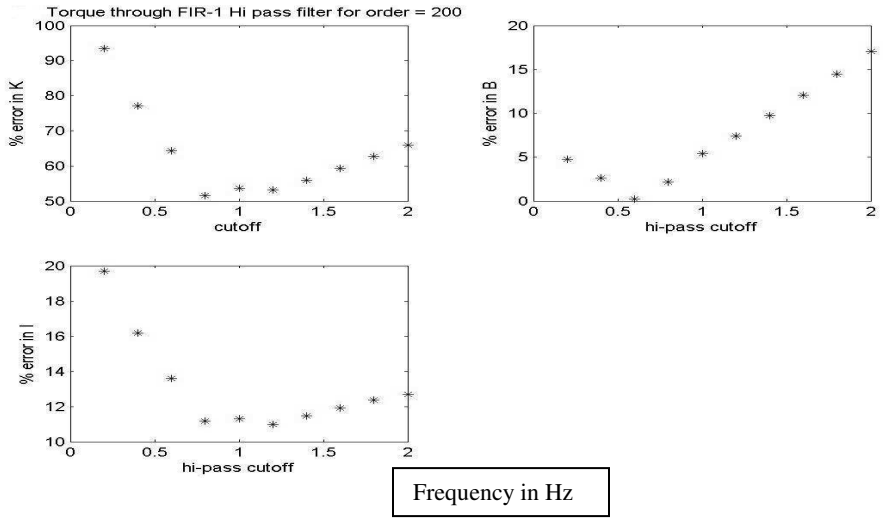

Figure 4-6 Estimation errors in the K, B and I when the simulated total torque is passed through a window-based FIR high pass filter of length 200 at various cut off frequencies.

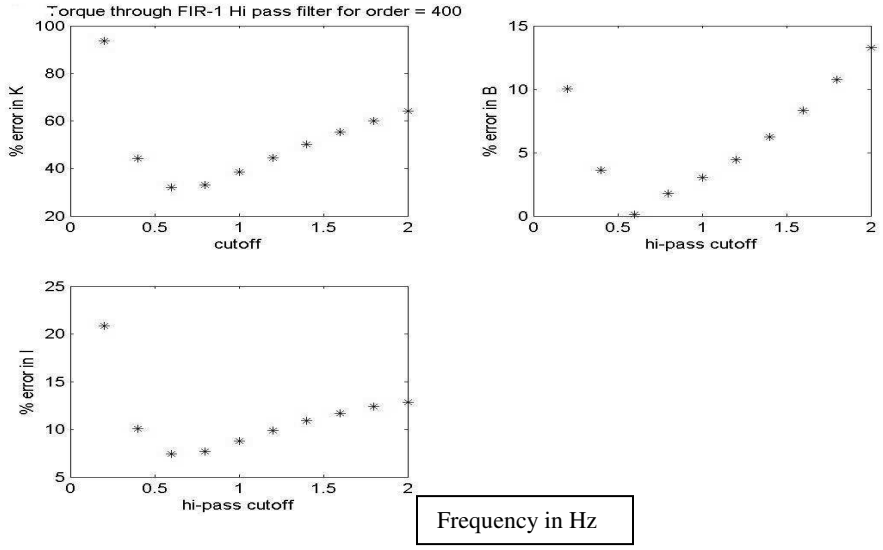

Figure 4-7 Estimation errors in the K, B and I when the simulated total torque is passed through a window-based fir high pass filter of length 400 at various cut off frequencies.

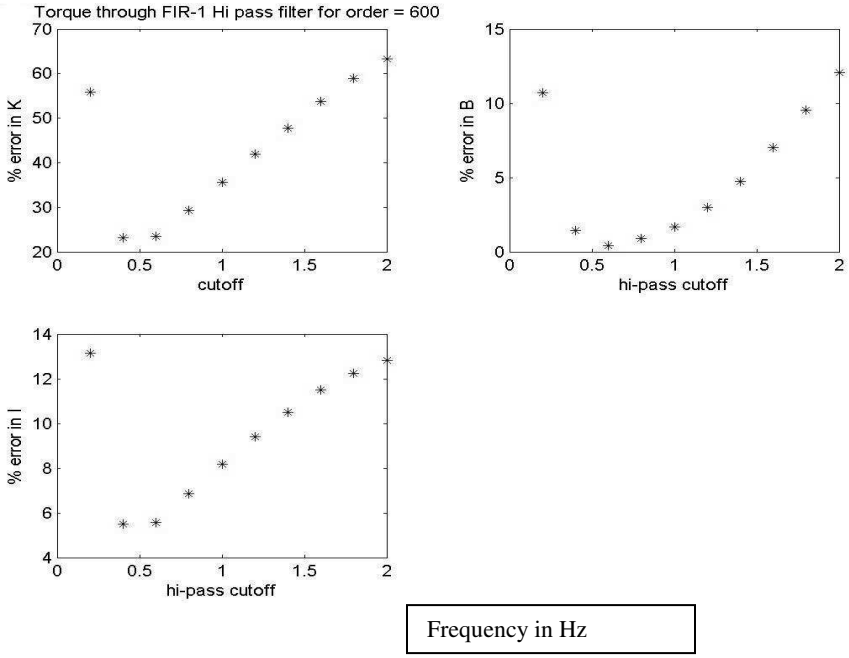

Figure 4-8 Estimation errors in the K, B and I when the simulated total torque is passed through a window-basedFIRhigh pass filter of length 600 at various cut off frequencies.

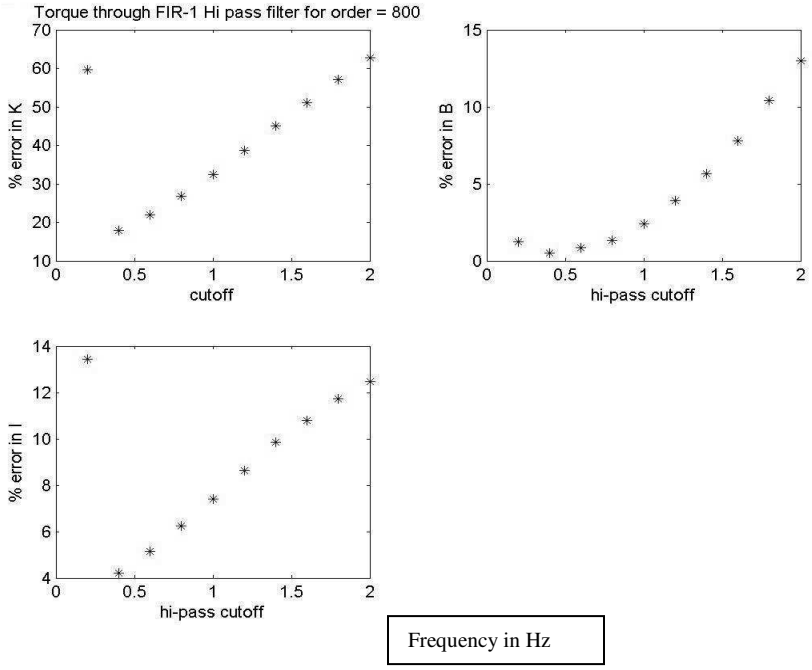

Figure 4-9 Estimation errors in the K, B and I when the simulated total torque is passed through a window-basedFIRhigh pass filter of length 800 at various cut off frequencies.

4.4.2 Linear Phase FIR- Least Squares Approach

Another approach tried was to use least squares linear phase FIR filter design. These linear phase FIR filters could provide sharper cut-offs at lower orders. In this way they could perform better than the window-based approach of FIR filters.

The total measured torque was passed through a linear phase FIR filter before estimating the parameters. The filters were of length 200, 400, 600 and 800 taps. Figure 4-10, Figure 4-11, Figure 4-12 and Figure 4-13 display plots of the percentage errors in K, B and I. We can observe from the plots that the error in estimating K is high while using any of these FIR filters, albeit the results are better than those when using the window design technique. As before, the increase in performance at higher orders comes at the expense of longer start-up transients (i.e. higher order filters). Therefore, a least squares FIR filter approach would not be appropriate to remove the torque bias.

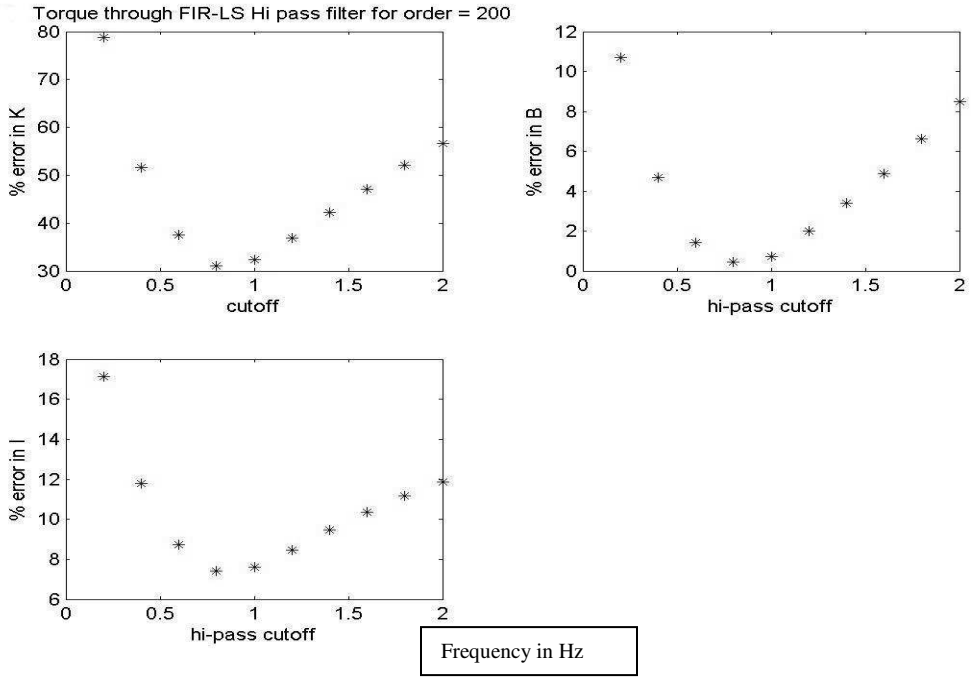

Figure 4-10 Estimation errors in the K, B and I when the simulated total torque is passed through a least squares FIR high pass filter of length 200 at various cut off frequencies.

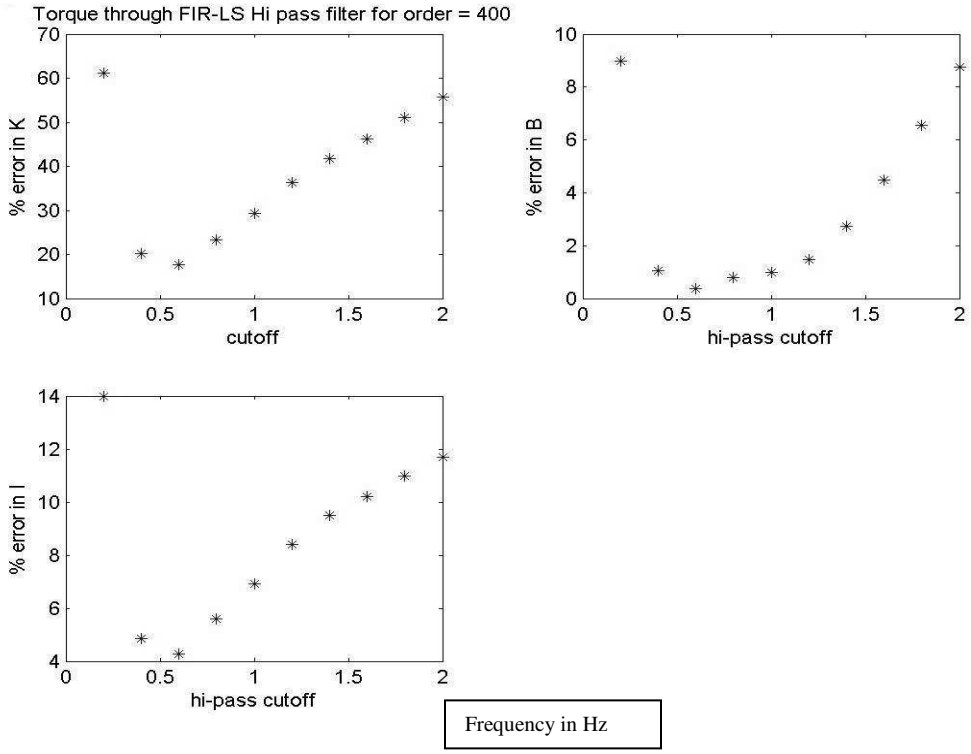

Figure 4-11 Estimation errors in the K, B and I when the simulated total torque is passed through a least squares high pass filter of length 400 at various cut off frequencies.

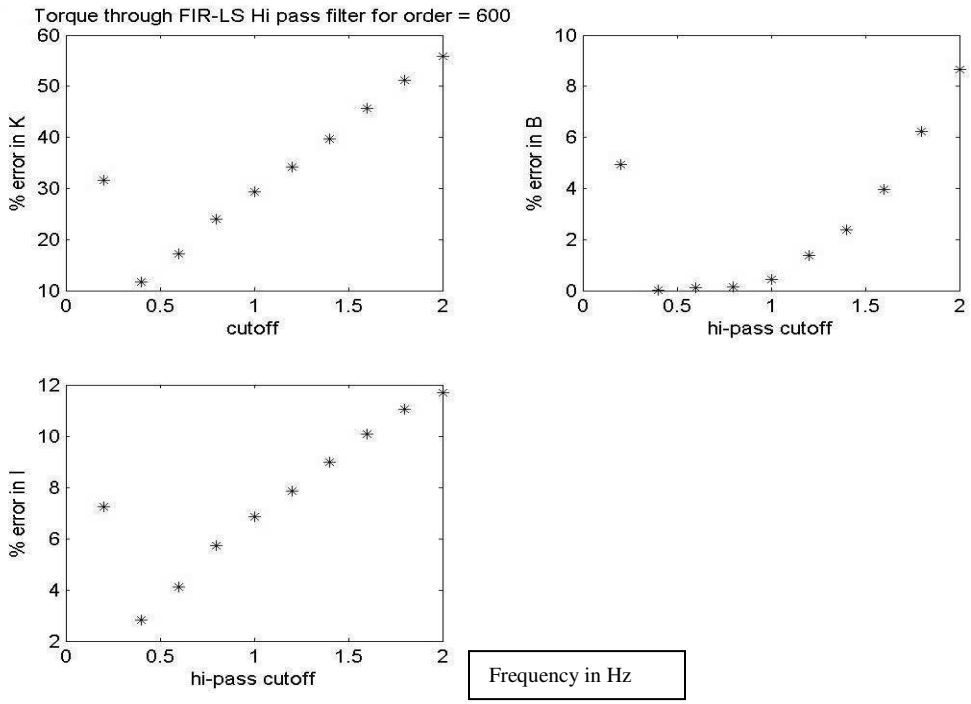

Figure 4-12 Estimation errors in the K, B and I when the simulated total torque is passed through a least squares FIR high pass filter of length 600 at various cut off frequencies.

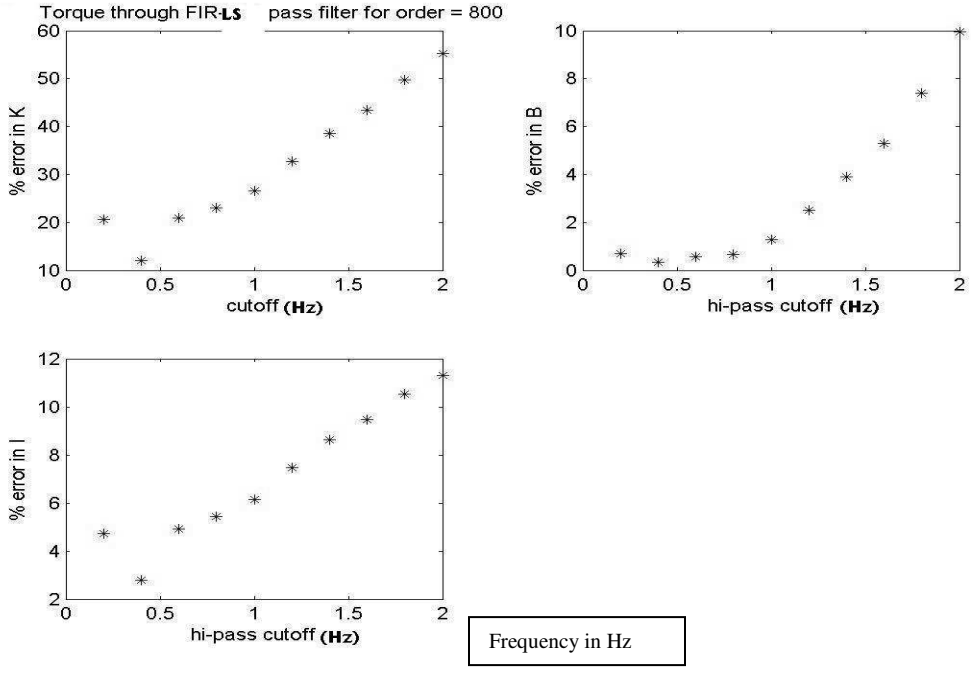

Figure 4-13 Estimation errors in the K, B and I when the simulated total torque is passed through a least squares high pass filter of length 800 at various cut off frequencies.

4.4.3 Butterworth Filters

Butterworth filters are infinite impulse response (IIR) filters which could also be used for removing the torque bias from the total torque measurement so that we can extract the ΔT signal. Butterworth filters could have shorter start-up transients which was a problem in the previous approach and could provide reduced error (previous approaches had errors of 20% in estimating K, using a low-pass cut-off frequency of 1 Hz).

Butterworth filters of order 2, 3 and 4 were investigated. Figure 4-14, Figure 4-15 and Figure 4-16 show us the results of the errors in calculating the impedance parameters when total torque is passed through the Butterworth filters. The error in evaluating the elastic parameter K did not improve considerably over the previous approaches. A 25% error is observed in estimating K with a cut-off as low as 1 Hz. It is clear from the errors that Butterworth filters are not an adequate approach to this problem of slowly varying torque.

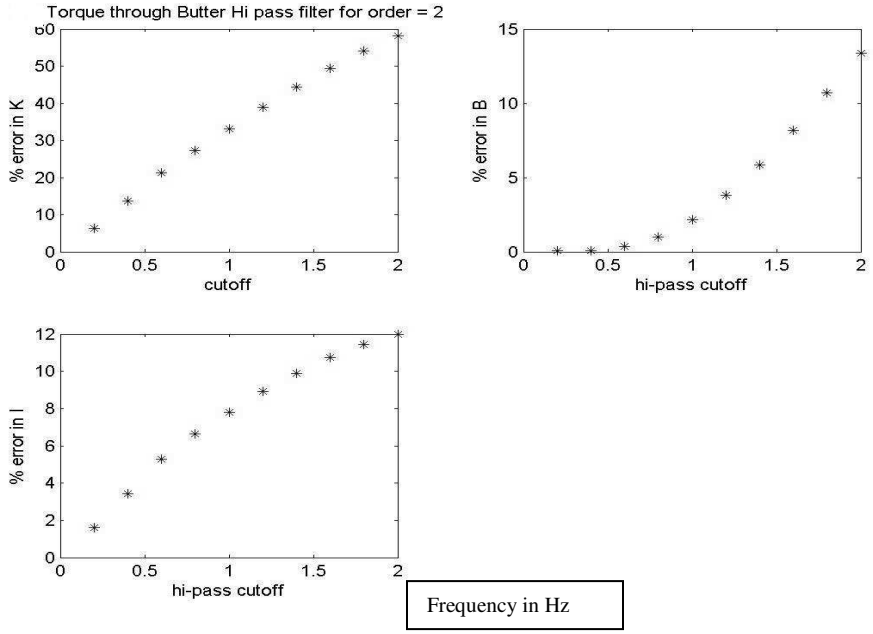

Figure 4-14 Estimation errors in the K, B and I when the simulated total torque is passed through a butter-worth high pass filter of order 2 at various cut off frequencies.

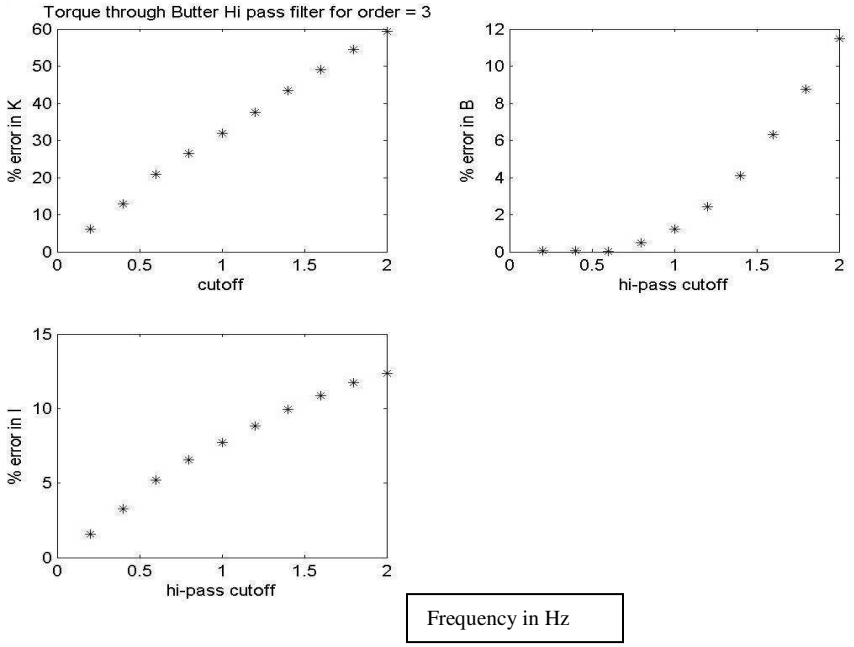

Figure 4-15 Estimation errors in the K, B and I when the simulated total torque is passed through a butter-worth high pass filter of order 3 at various cut off frequencies.

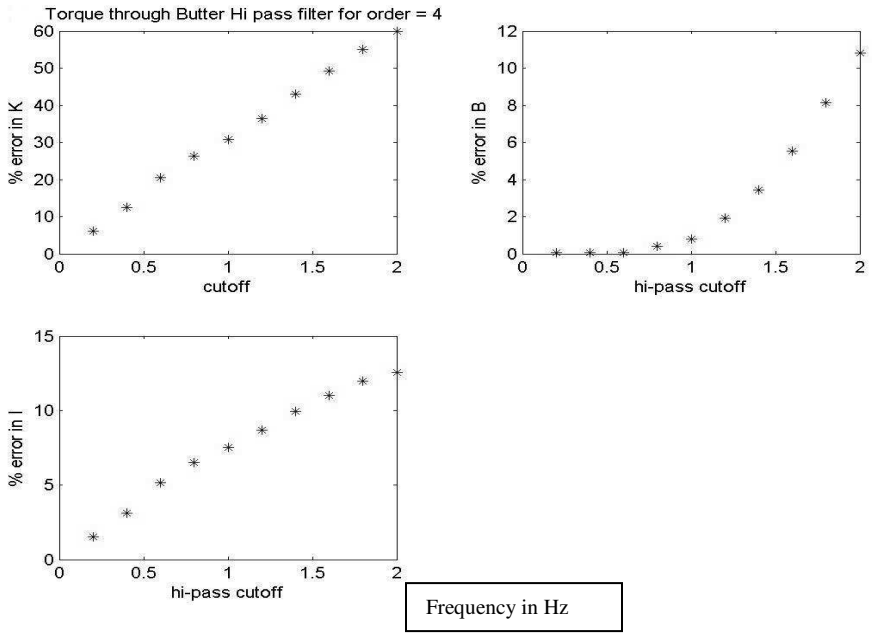

Figure 4-16 Estimation errors in the K, B and I when the simulated total torque is passed through a butter-worth high pass filter of order 4 at various cut off frequencies.

4.4.4 Polynomial Subtraction

Removing the best fit line or the best fit polynomial from the measured torque is another approach to remove the torque bias. The best-fit polynomial would ideally correspond to the slowly varying component in the measured total torque signal. Therefore, we fit a polynomial to the measured torque and then subtracted that polynomial from the measured torque.

Figure 4-17 shows the results of these simulations as a function of polynomial degree, and it is clear that the errors in estimation are considerably reduced (compared to the linear filtering techniques) when this approach is chosen. The error in estimating K has dropped to just about 2% even when a third degree polynomial is subtracted from the measured torque. There are no start-up transients when we choose this approach over the filtering approach. Therefore, no data would be lost with the start-up transients, when we use this approach.

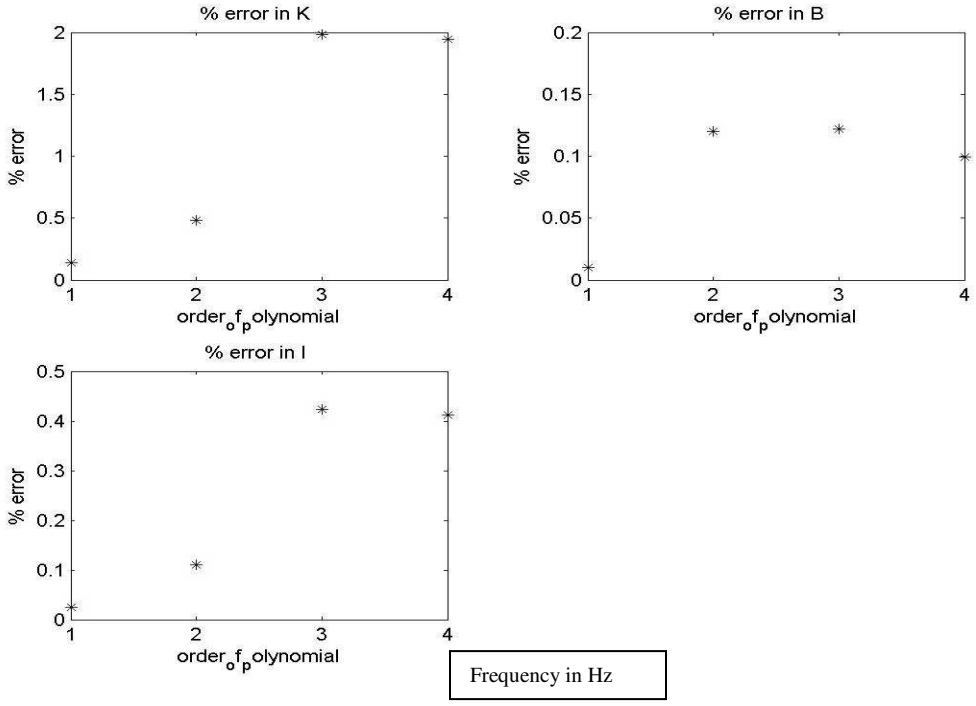

Figure 4-17 Estimation errors in the K, B and I when a best fit polynomial is subtracted from the simulated total torque before estimating the impedance parameters.

The same methods were now tried on a simulated torque that has a torque bias varying as a ramp instead of a constant torque. Figure 4-18 and Figure 4-19 give us the results when we use a window based FIR filter. The errors in estimating K are quite high. When the least squares FIR filter design approach was used, shown in Figure 4-20 and Figure 4-21, results are also unsatisfactory. Subtracting out the best fit polynomial, shown in Figure 4-22, reduces the errors considerably to acceptable levels. The plots show that we have tried subtracting out the polynomials of degree up to 14. The best fit polynomial to be subtracted can only be decided after evaluating experimental data sets, since the nature of the experimental torque bias drift is not well understood. The simulations have shown that this method (of polynomial subtraction) works better than high-pass filtering.

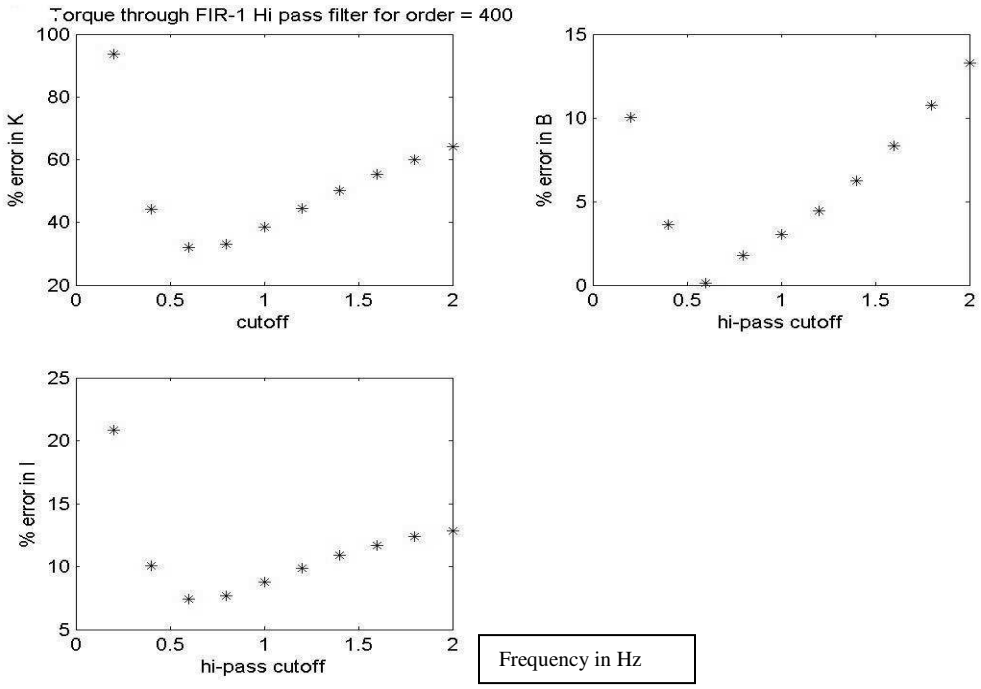

Figure 4-18 Estimation errors in the K, B and I when the simulated total torque is passed through a window based FIR high pass filter of length 400 at various cut off frequencies.

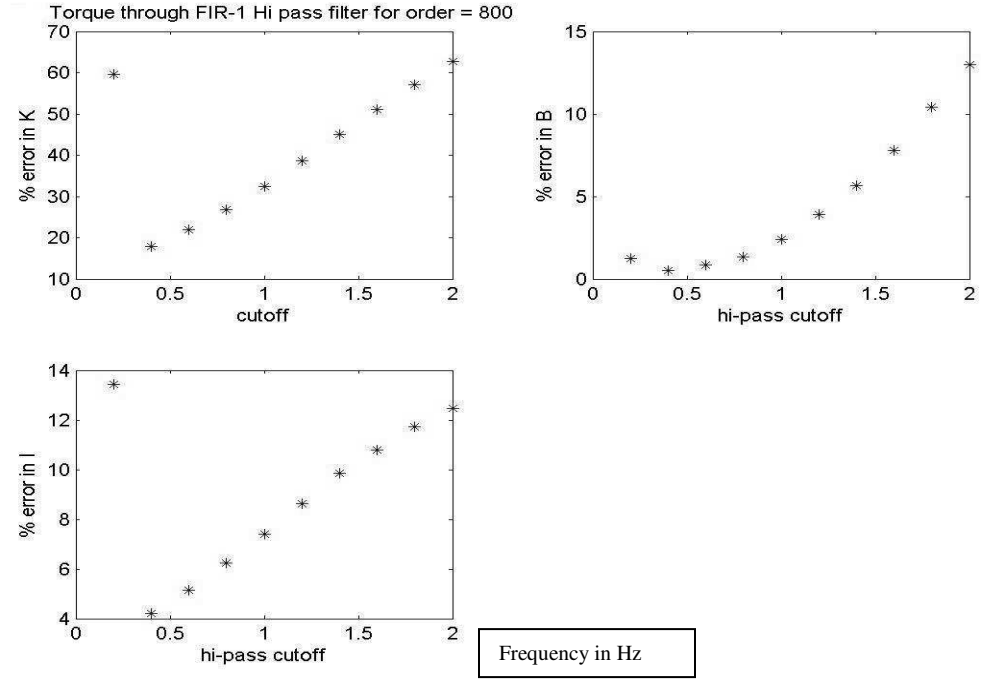

Figure 4-19 Estimation errors in the K, B and I when the simulated total torque is passed through a window based FIR high pass filter of length 800 at various cut off frequencies.

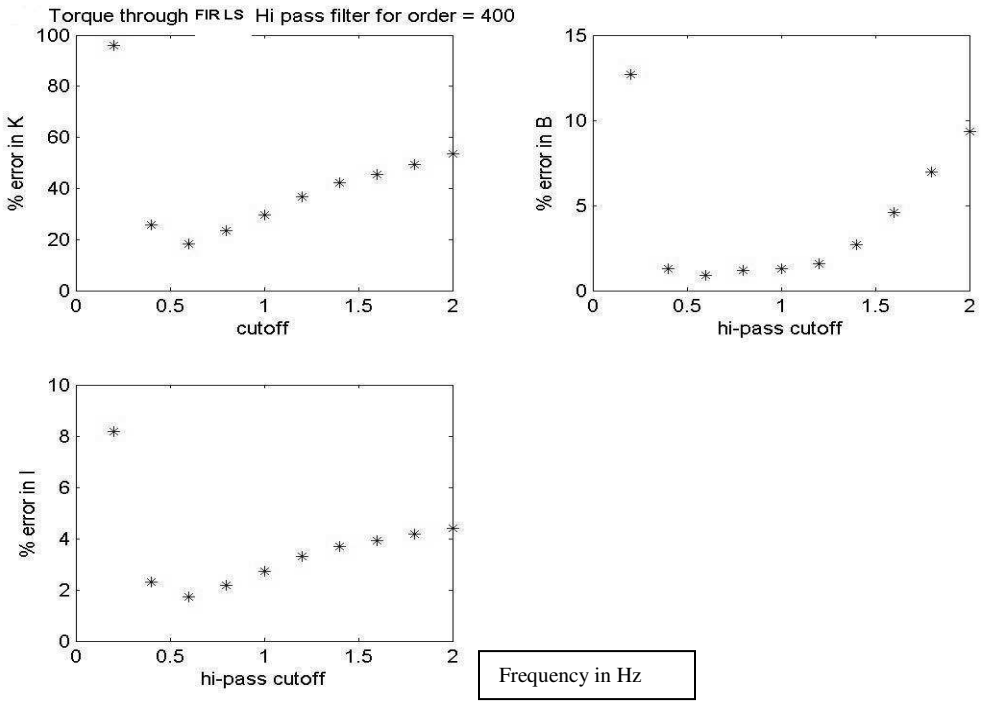

Figure 4-20 Estimation errors in the K, B and I when the simulated total torque is passed through a least squares FIR high pass filter of length 400 at various cut off frequencies.

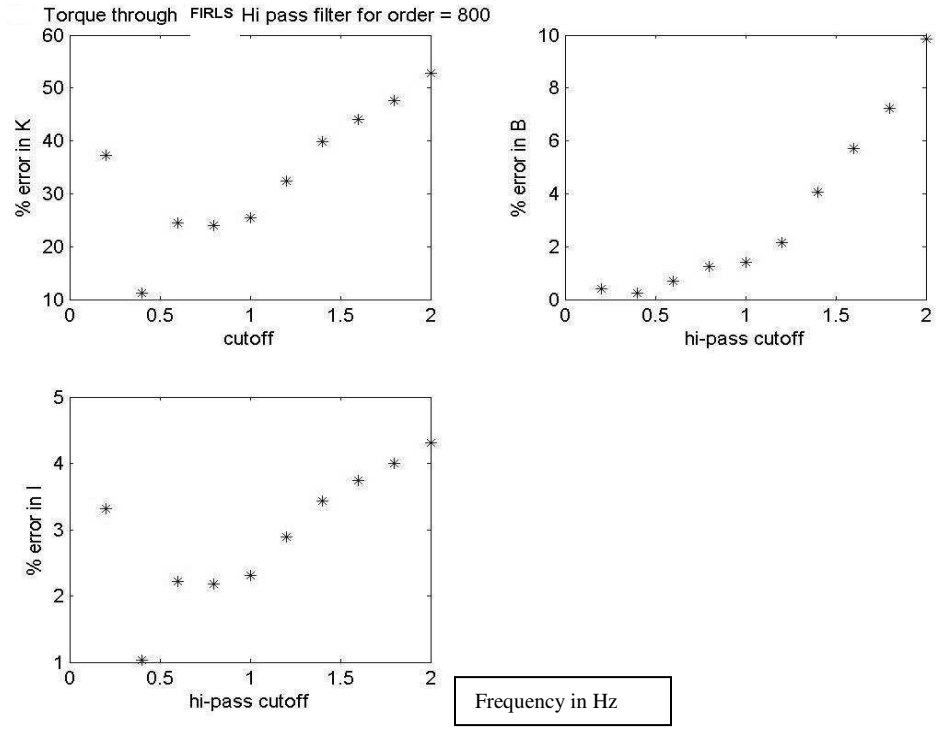

Figure 4-21 Estimation errors in the K, B and I when the simulated total torque is passed through a least squares based FIR high pass filter of length 800 at various cut off frequencies.

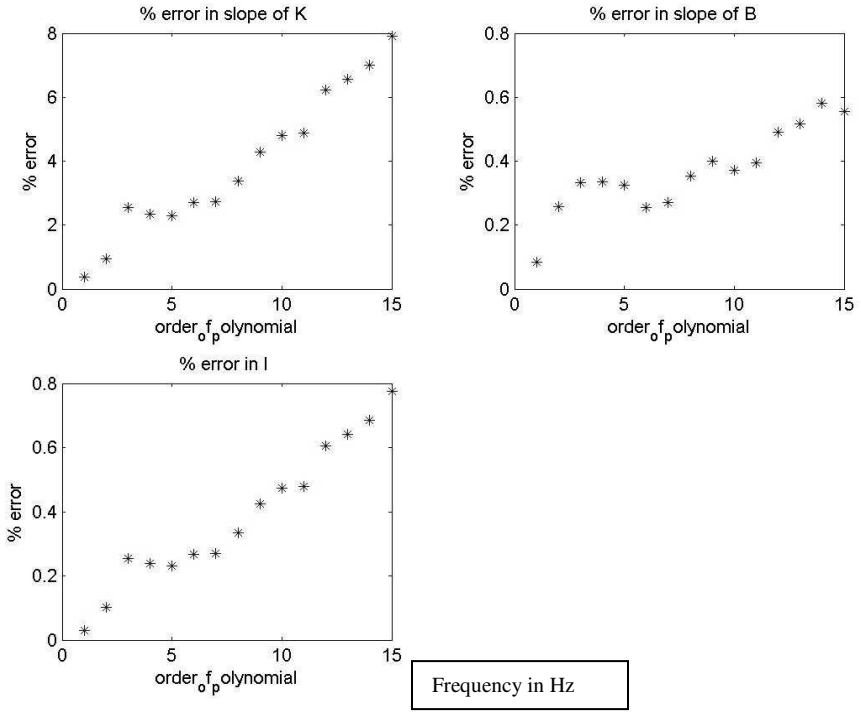

Figure 4-22 Estimation errors in the K, B and I when a polynomial is subtracted from the simulated total torque before estimating the impedance parameters.

4.5 Estimation Using EMG Amplitude

Our intention with this project was to estimate the impedance parameters (K, B, I) using EMG. Simulations were performed to find out what duration data need be collected and the effect of noise (in EMG amplitude estimates) on estimation of the impedance parameters.

4.5.1 Model Equation

For slowly-force varying perturbation trials, the experimental state is a function of the EMG amplitude estimates ($\hat{s}_E, \hat{s}_F$). The second order linear equation relating EMG amplitude and change in angular displacement to the change in torque produced about the joint is modeled as:

$$\Delta T = K(\hat{s}_E, \hat{s}_F) \cdot \Delta\theta + B(\hat{s}_E, \hat{s}_F) \cdot \Delta\dot{\theta} + I \cdot \Delta\ddot{\theta}$$

Equation 4-6

where

$\hat{s}_E$ is the EMG amplitude estimate of the extensor muscles,

$\hat{s}_F$ is the EMG amplitude estimate of the flexor muscles,

$\Delta\theta$ is the change in angular displacement of the joint,

ΔT is the change in torque produced about the joint.

$K(\hat{s}_E, \hat{s}_F)$ is the elastic stiffness function,

$B(\hat{s}_E, \hat{s}_F)$ is the viscosity function and

I is the constant inertial parameter.

We select

$$K(s_E, s_F) = k_e \hat{s}_E + k_f \hat{s}_F \text{ and}$$

Equation 4-7

$$B(\hat{s}_E, \hat{s}_F) = b_e \hat{s}_E + b_f \hat{s}_F$$

Equation 4-8

Making these selections (as in Equation 4-7 and Equation 4-8) is advantageous for two reasons. First, the elastic (K) and viscous (B) functions are now linear functions of EMG amplitude estimates ($\hat{s}_E, \hat{s}_F$) and can be estimated with the use of linear least squares. Second, we know that EMG amplitudes increase with increase in background joint torque [3] and so do the elastic and viscous parameters [13]. Thus we can have a model where K and B increase with EMG amplitudes. Our conditions are a quasi-constant operating point and the variations in K and B should be consistent with those reported in the literature. A polynomial increase in K and B is reasonable according to

data collected by Kearney and Hunter [7]. For the work described in this project, we assume a first degree polynomial relation. Later studies can involve higher degree polynomials. We also know that K and B vanish with zero torque bias [13] and therefore we omit the bias portion of the polynomial. The elastic function K and viscous function B are varying quantities (vary with change in activation level of the muscle), while I is a constant quantity since the inertial term does not change appreciably for different activation levels of the muscle. The terms k_e, k_f, b_e, b_f and *I* are the fit parameters for the linear least squares technique.

The purpose of these simulations was to investigate the amount of data that need be collected in order to be able to estimate impedance accurately. Although previous experiments have been performed [7] where impedance parameters have been estimated using Equation 4-1, there is a need to perform a different set of simulations for this new model. Here, the impedance parameters are estimated from EMG amplitude estimates which are by themselves noisy. The position measurements, θ, are taken from a quantizer, due to which the first and second derivatives, $\dot{\theta}$ and $\ddot{\theta}$, have high frequency noise associated with them [see section 4.2] which are multiplied by the EMG inputs which leads to the input noise being accumulated. There are more fit parameters (five) here as opposed to Equation 4-1 (three).

4.5.2 Simulation Method

The simulated relation between background torque and K (or B) and the associated torque bias was taken from [13]. The first step was to generate (simulate) all the measurements acquired during an experiment as in Figure 4-23 and thereafter to

estimate the impedance parameters using these measurements as in Figure 4-24. The estimated parameters were then compared against the simulated values.

Generation of the signals consists of the following steps, shown in Figure 4-23:

1. Generating the angular measurements ($\Delta\theta$) as a band-limited Gaussian random signal (section 4.1.2).
2. Ideal EMG amplitudes for the flexor and extensor muscles are selected as a profile that varies linearly from 50% MVC flexion to 50% MVC extension.
3. ke, kf, be, bf and I are selected so that we get realistic values of $K(\hat{s}_e, \hat{s}_f)$ and $B(\hat{s}_e, \hat{s}_f)$ as in Rymer's work [13] (subject S and Z selected from Rymer's work).
4. Random Gaussian noise (the standard deviation of the noise varied as described below) was added to the EMG amplitudes, the standard deviation of which increases with the EMG amplitude estimate itself [14,15]. Noisy EMG amplitudes are used instead of raw EMG itself.
5. ΔT (change in torque) was generated using Equation 4-6 and the previously simulated information.
6. Torque bias was generated as a ramp for the corresponding values for K(t) and B(t) from step 3 using [13].
7. The torque bias was added to ΔT to obtain the total torque measurement.

The above set of steps returned the total torque, position measurements and the noisy EMG amplitudes. These measurements were used by the parameter estimation module. Noisy EMG amplitudes are used instead of raw EMG itself.

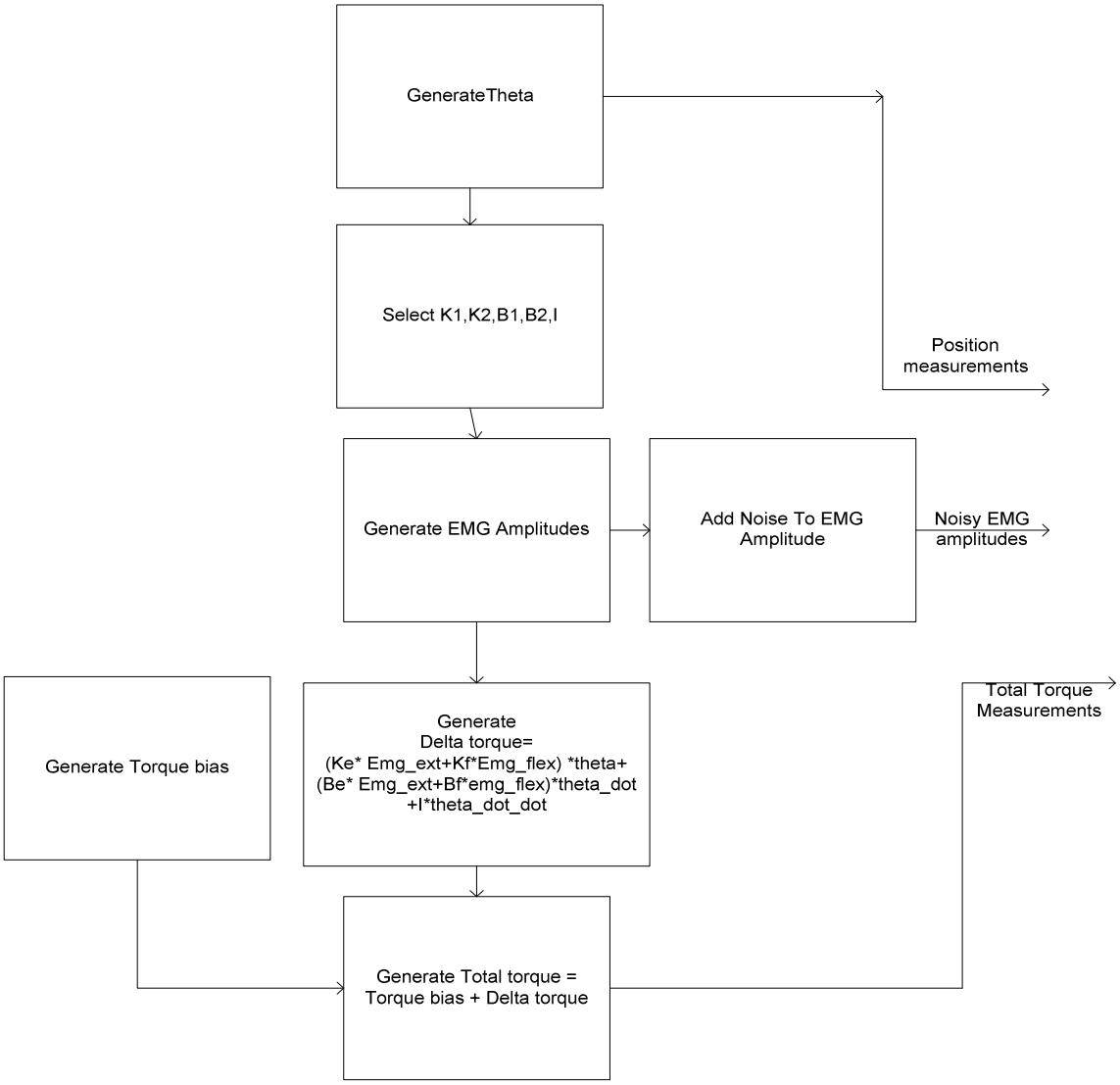

Figure 4-23 Generation of measurement signals for simulation

The parameter estimation module carried out the following steps, as depicted in Figure 4-24:

1. Remove the torque bias from the total-torque measurements to get ΔT, using the first-degree polynomial subtraction technique (section 4.4.4) .
2. Subtract the mean bias from the position measurements (to get $\Delta\theta$).
3. Use ΔT , $\Delta\theta$ and the noisy EMG amplitude estimates to estimate ke, kf, be, bf and I using linear least squares.

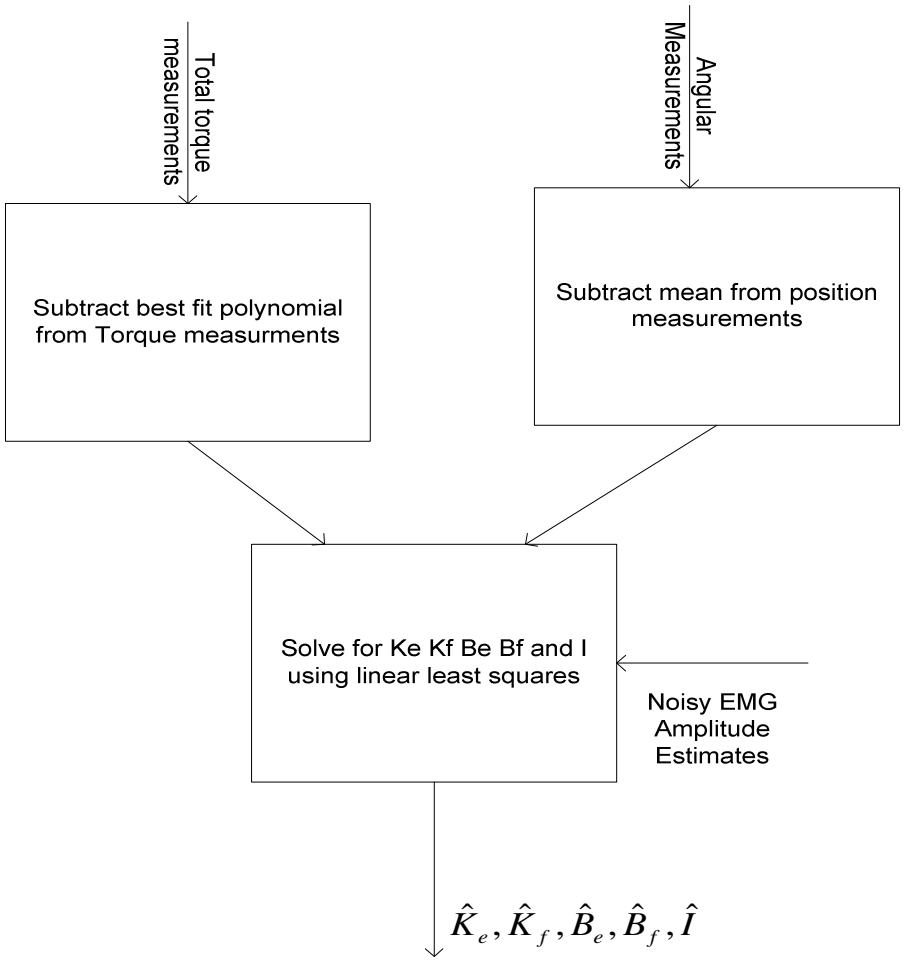

Figure 4-24 Parameter Estimation module

4.5.3 Simulation Waveforms and Results

The generated angular deviations ($\Delta\theta$), as seen in Figure 4-25, were the input to the system and were generated as described in section 4.1.2.

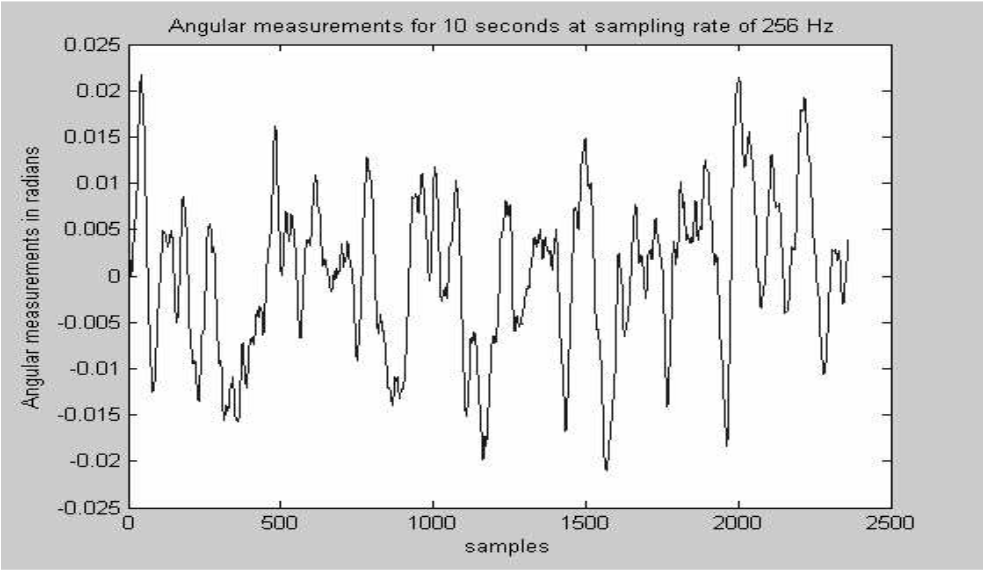

Figure 4-25 Angular deviations at a sampling rate of 256 Hz.

The values for the background bias torque were taken from Rymer's work [13] and varied as a ramp from 50% MVC flexion to 50% MVC extension (Figure 4-26)

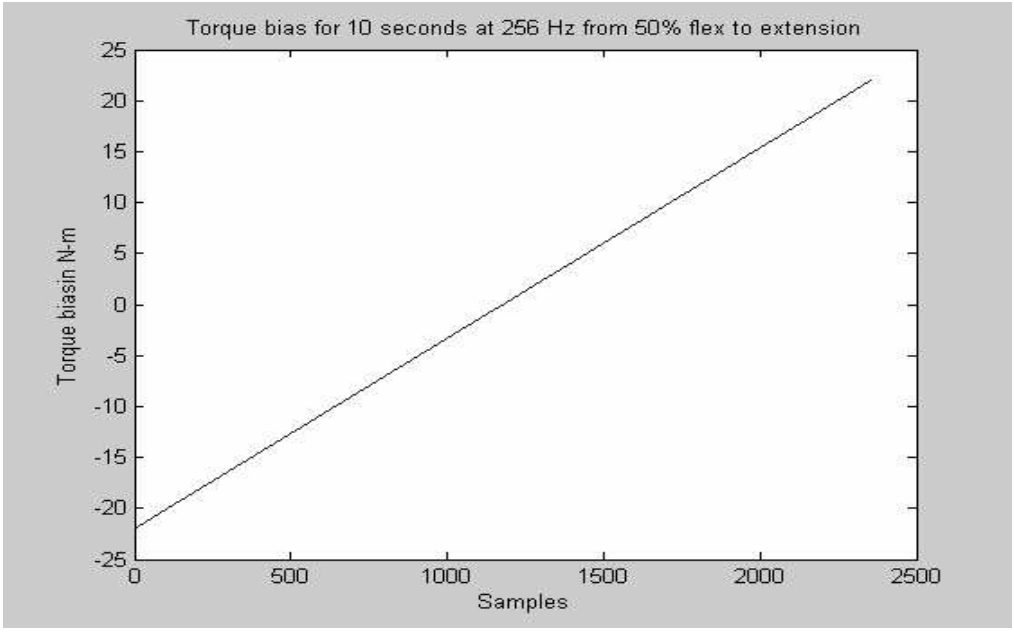

Figure 4-26 Background torque bias (in N-m) varying as a ramp, sampling rate of 256 Hz used.

Figure 4-27 and Figure 4-28 show the noisy EMG extensor amplitude and the EMG flexor amplitude respectively. The EMG amplitude estimates shown were assigned a signal to noise ratio (SNR) of 5. The standard deviation of the EMG amplitudes increase with the increase in the mean EMG amplitude [14].

$$SNR_{emg} = \frac{\mu(t)}{\sigma(t)}$$

Equation 4-9

where $\mu(t)$ is the time varying mean of the EMG amplitude and $\sigma(t)$ is the standard deviation. The noise is white Gaussian multiplied by $\sigma(t)$. On the y-axis, 1 represents MVE (maximum voluntary EMG).

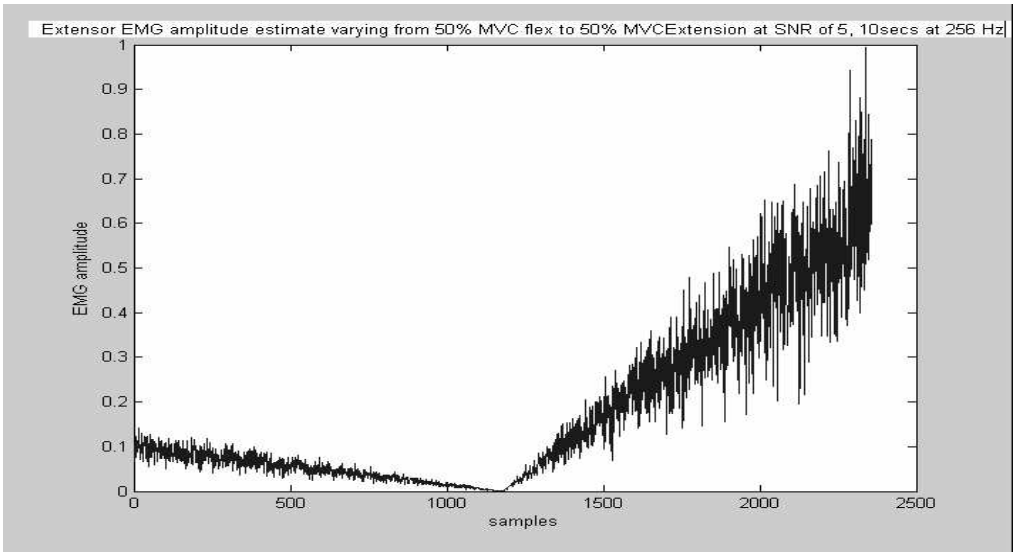

Figure 4-27 Extensor EMG amplitude (noise varying as a function of the amplitude) varying from 50% MVC flexion to 50%MVC extension, sampling rate of 256 Hz used.

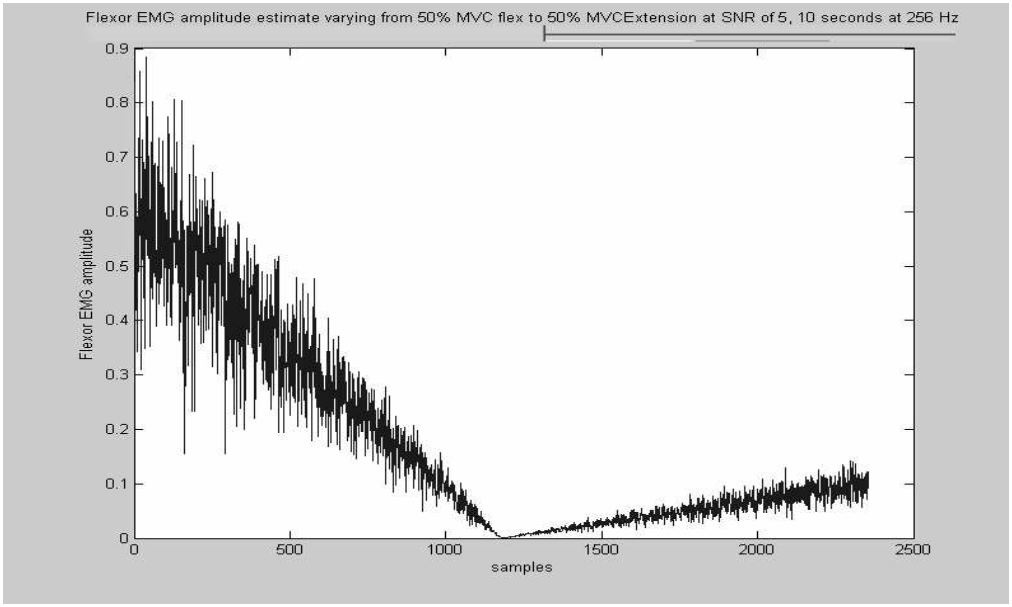

Figure 4-28 Flexor EMG amplitude (noise varying as a function of the amplitude) varying from 50% MVC flexion to 50%MVC extension, sampling rate of 256 Hz.

Figure 4-29 shows the total torque generated when we use $K(\hat{s}_E, \hat{s}_F)$ and $B(\hat{s}_E, \hat{s}_F)$ (as in Figure 4-30), I = 0.113, $\Delta\theta$ (as in Figure 4-25), EMG extension and flexion (as in Figure 4-27 and Figure 4-28) in Equation 4-6.

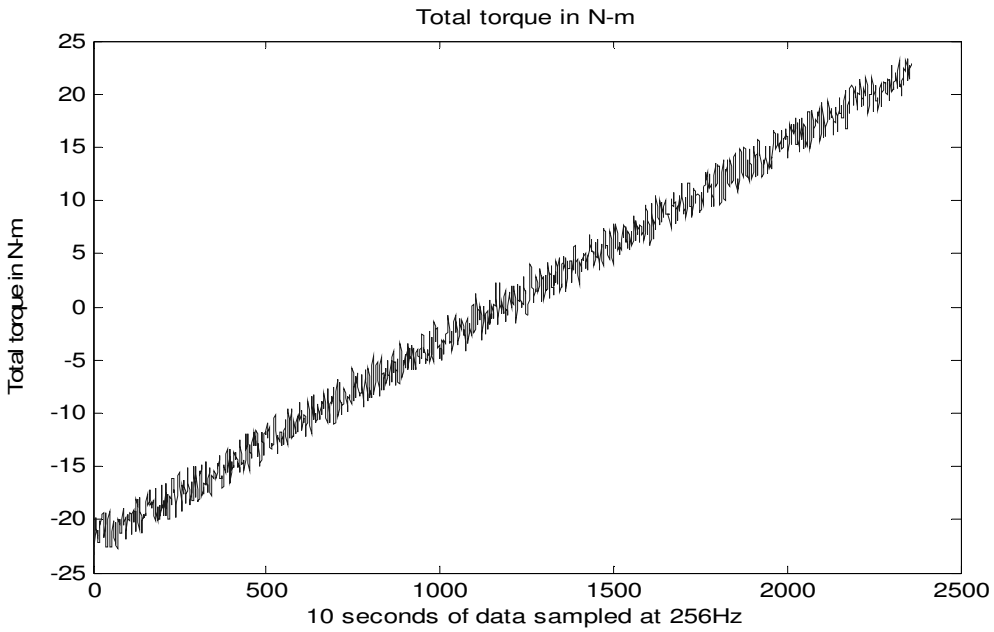

Figure 4-29 Generated total torque (in N-m). Data collected for 10 seconds at the rate of 256 Hz.

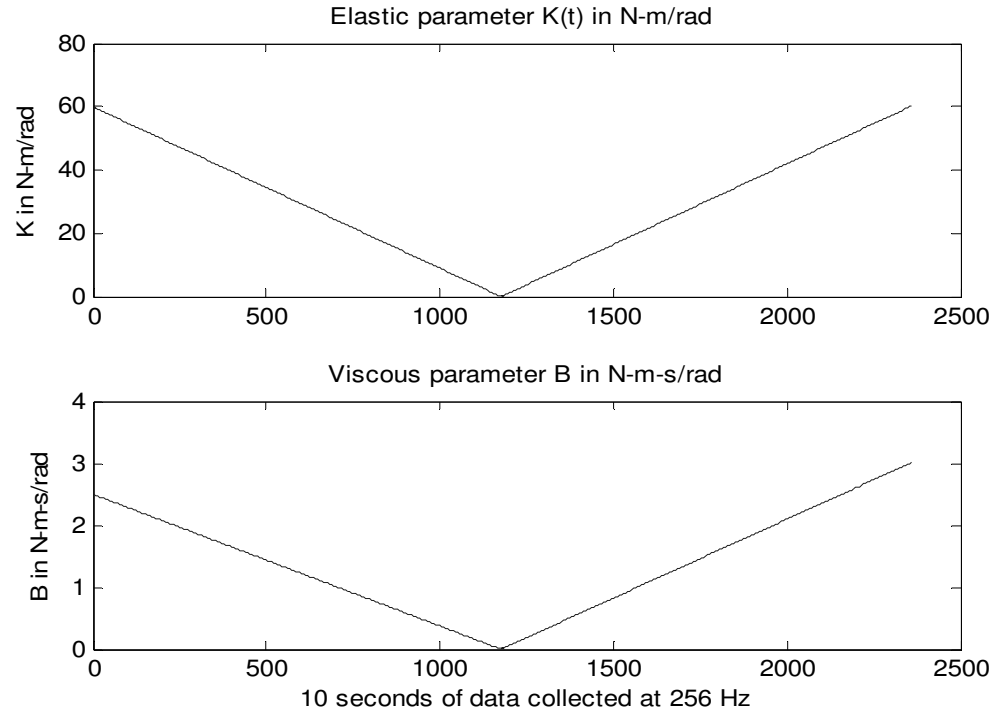

Figure 4-30 Simulated values of K(t) and B(t) with bias torque varying from 50% MVC flexion to 50% extension

The generated signals were then used to estimate the impedance parameters. The simulation was carried out for lengths of data sets varying from 10 seconds to 40 seconds and for varying EMG SNR's (5, 15 and 25). The background torque and EMG amplitude were varied from 50% flexion to 50% extension irrespective of the length of the data set chosen. A data set shorter in length had values ramping up faster than that of a longer data set. After estimation, the error was calculated between the actual impedance parameters and the estimated values. Each simulation condition was repeated 50 times, using distinct random values each time. Figure 4-31 shows a plot of the mean plus-and-minus standard deviation of the percentage errors in estimating $ke, kf, be \text{ and } bf$, where

$$\%Error\ in\ estimation = \frac{Kactual - Kestimate}{Kactual} * 100$$

Equation 4-10

.

For this calculation, Kactual is the simulated value of the elastic parameter K and Kestimate is the estimated K after linear least squares. Errors are plotted for various lengths of data sets starting from 10 seconds to 40 seconds. The various plots represent different SNR for EMG used for estimation (solid line with square markers represents EMG amplitudes with an SNR of 5, dotted line with triangle markers an SNR of 15 and solid line with circular markers an SNR of 25). Figure 4-31and Figure 4-32 show that the error is high for a data set of 10 seconds and then drops considerably for longer data sets. We can also observe that the error reduces with better EMG SNR. The performance (low errors) for ke, kf, be, bf and I are quite within acceptable limits for data sets of 20 seconds or more. From the plots, we can say that the system identification requires a

minimum length of data of 20 seconds for good performance and that a data set of 10 seconds is not sufficient. The elastic parameter *ke* is most susceptible to short data durations.

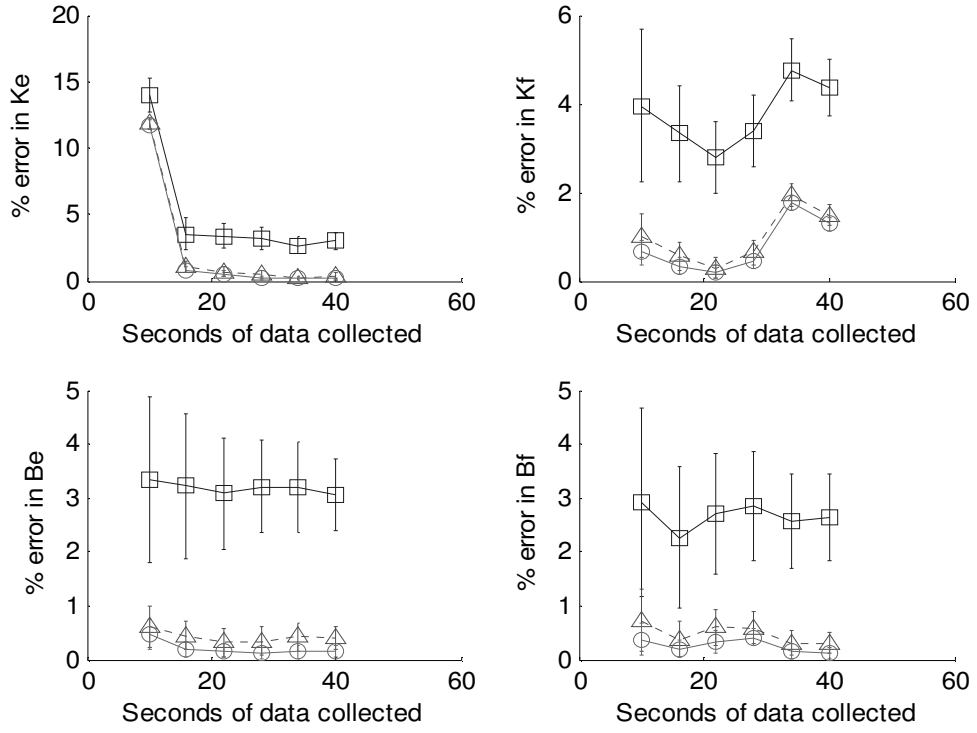

Figure 4-31 Mean ± standard deviation percentage errors in estimating $ke, kf, be \text{ and } bf$. The solid line with square markers represents EMG amplitudes with SNR of 5, dotted line with triangle markers SNR of 15 and solid line with circular markers being SNR of 25.

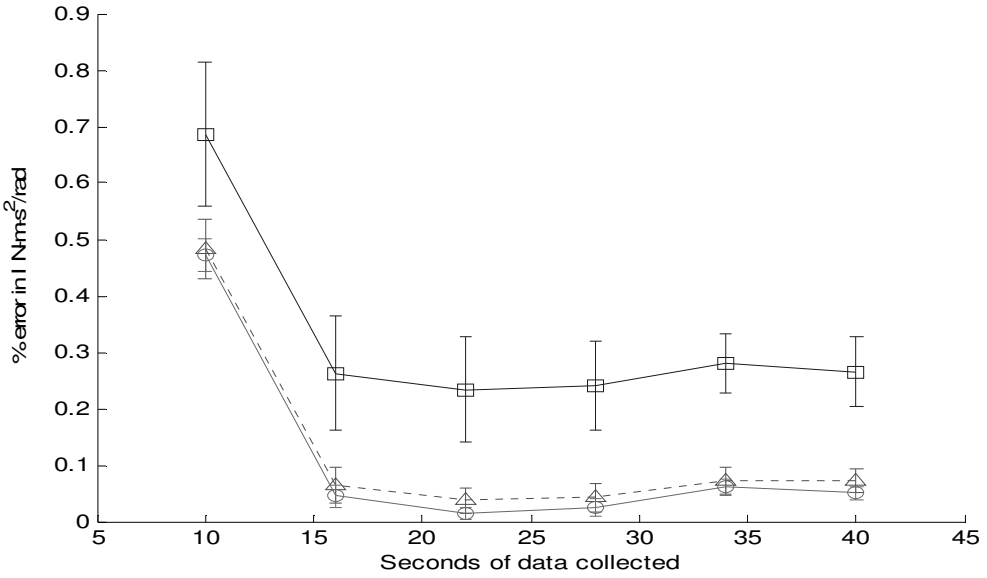

Figure 4-32 Mean ± standard deviation percentage errors in estimating I, the solid line with square markers represents EMG amplitudes with SNR of 5, dotted line with triangle markers SNR of 15 and solid line with circular markers being SNR of 25.

Figure 4-33 displays a plot of mean ± standard deviation error in root mean square (RMS) for $K(\hat{s}_E, \hat{s}_F)$ and $B(\hat{s}_E, \hat{s}_F)$.

$$RMS\ error\ in\ K = \sqrt{\frac{\sum_{\forall i}(Kactual_i - Kestimate_i)^2}{N}},$$

Equation 4-11

where Kactual is the simulated value of $K(\hat{s}_E, \hat{s}_F)$ as in Figure 4-30, and Kestimate is its estimated value. N is the total number of sample times simulated. The plot shows that the mean RMS error is within 1% for both K and B for when the SNR of the EMG is 15 and above.

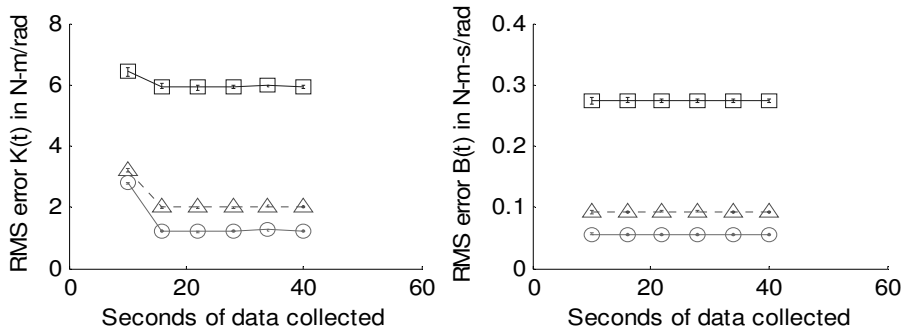

Figure 4-33 Mean ± standard deviation of RMS error in estimating K(t) and B(t) the solid line with square markers represent EMG amplitudes with SNR of 5, dotted line with triangle markers SNR of 15 and solid line with circular markers being SNR of 25.

A second set of simulations were performed with torque-varying background torque. These simulations were performed using parameter values taken from another subject (subject Z) from Rymer's work [13] (with different impedance and torque bias values). These values would help us calculate the error for other trials (or subjects), and to validate the simulations. Figure 4-34 shows a plot of the generated total torque (with bias torque varying from -40 N-m to 40 N-m) by another subject and the corresponding impedance parameter plots are shown in Figure 4-35. Figure 4-36, Figure 4-37 and Figure 4-38 show plots of the errors for the impedance parameters. The mean errors for the parameters are well under 2% for data sets of 20 seconds or longer at a sampling rate of 256 Hz for and an EMG SNR of 15.

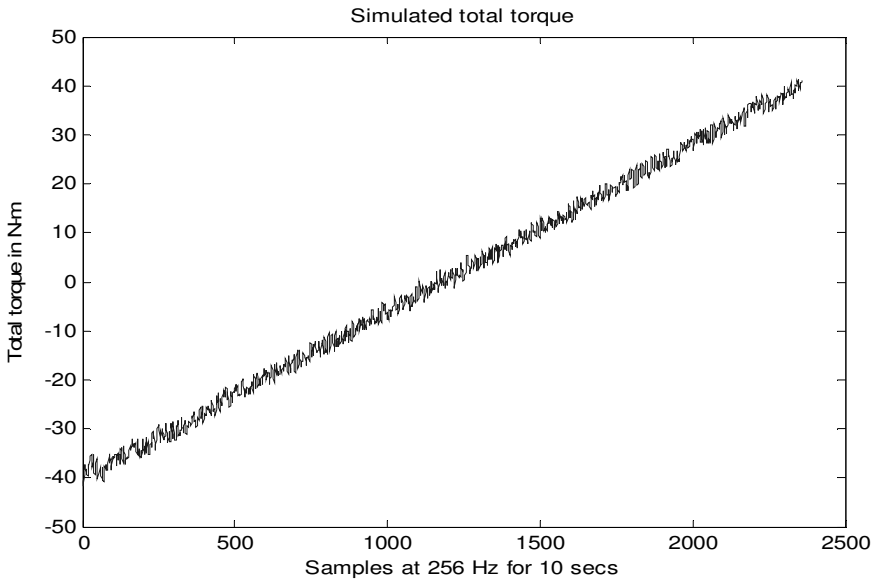

Figure 4-34 Generated total torque (for simulated subject 2) (in N-m). Data collected for 10 seconds at a sampling rate of 256 Hz.

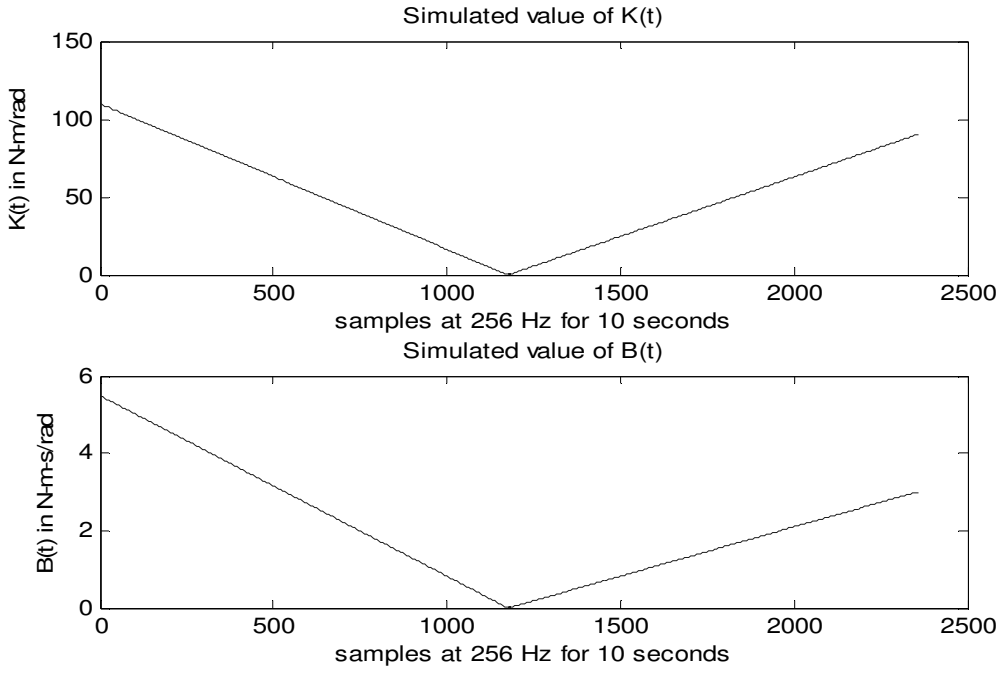

Figure 4-35 Simulated values of K(t) and B(t) (for subject 2) with bias torque varying from 50% MVC flexion to 50% extension

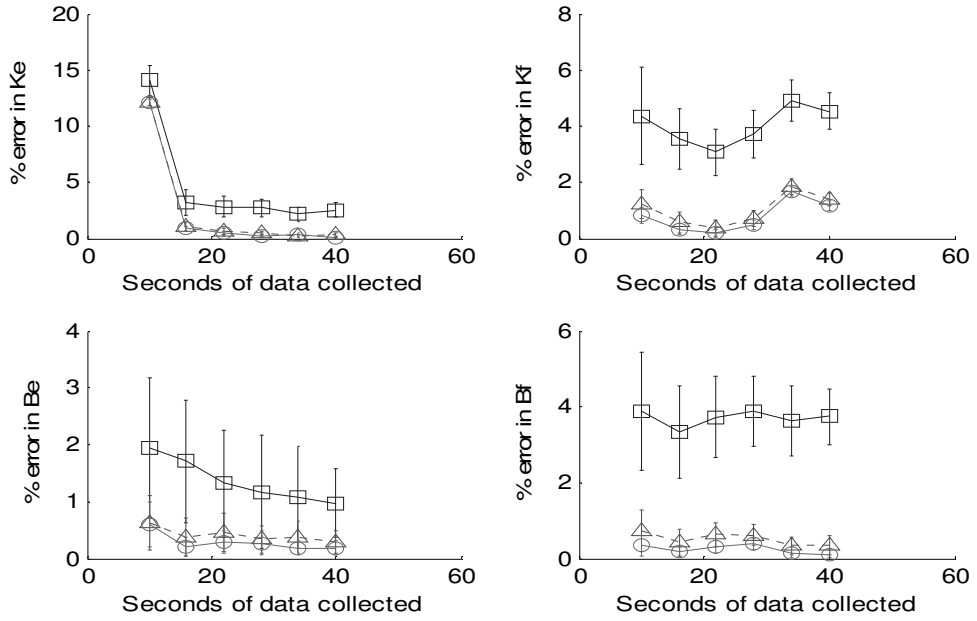

Figure 4-36 Percentage error in estimating Ke, Kf, Be, Bf the solid line with square markers represent EMG amplitudes with SNR of 5, dotted line with triangle markers SNR of 15 and solid line with circular markers being SNR of 25 (Subject 2 of Rymer's work [13]).

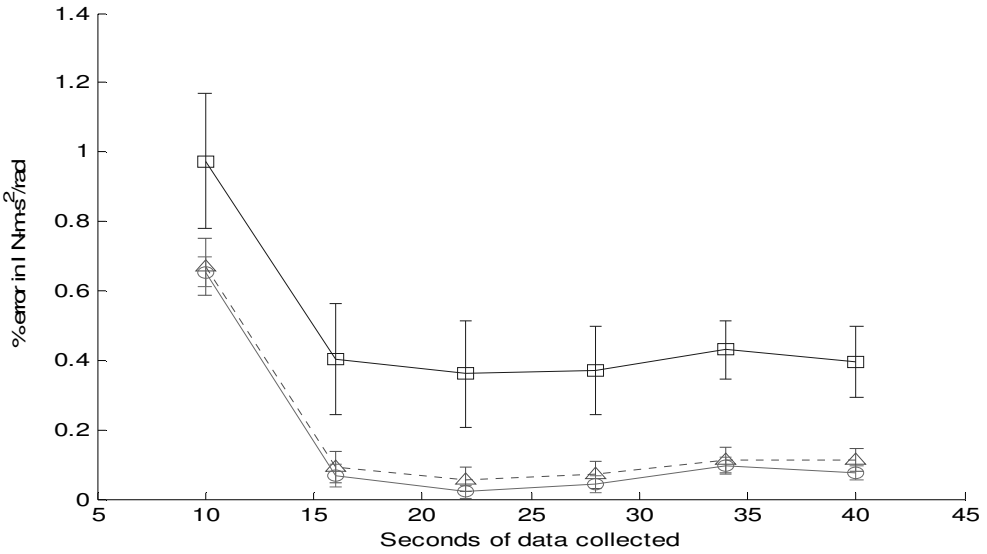

Figure 4-37 Percentage error in estimating I, the solid line with square markers represent EMG amplitudes with SNR of 5, dotted line with triangle markers SNR of 15 and solid line with circular markers being SNR of 25 (Subject 2 of Rymer's work [13]).

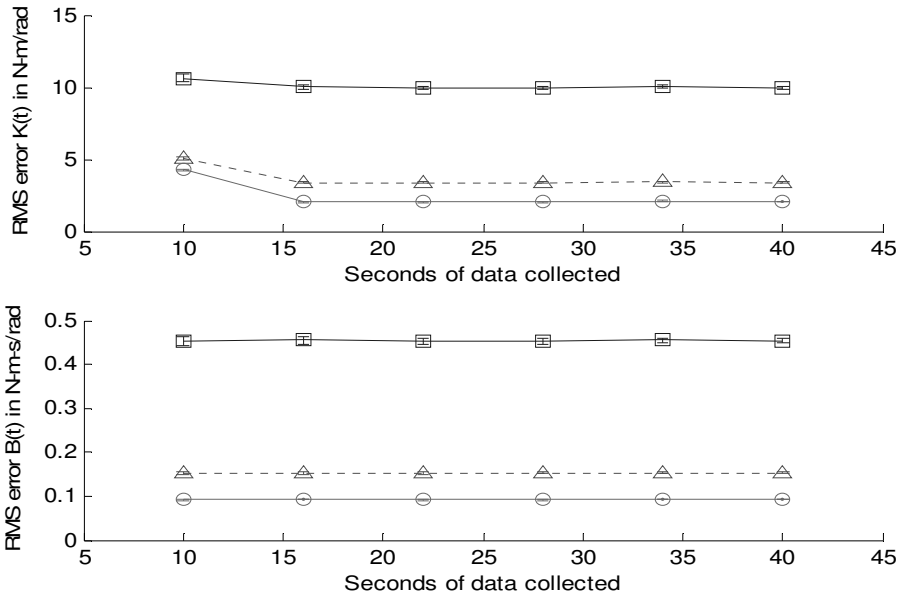

Figure 4-38 RMS error in estimating K(t) and B(t), the solid line with square markers represent EMG amplitudes with SNR of 5, dotted line with triangle markers SNR of 15 and solid line with circular markers being SNR of 25 (Subject 2 of Rymer's work [13]).

These simulations helped us find out how much data would need to be collected to achieve low error while estimating the impedance parameters (K, B and I). Using the simulations, we could infer that acquiring 30 seconds of data would be adequate for system identification with the assumptions inherent in the model. We can see that the errors in Kf and Bf increase by 0.5 % from 28 to 34 seconds. We would have expected the errors to reduce monotonically as the length of data set increased. The exact reason for the increase in error could not be analyzed at this time. Since the total amount of error was low, at both 28 and 34 seconds, we can be assured that we would have a good system identification process in place.

5 EXPERIMENTAL METHODS and RESULTS

5.1 Experimental Apparatus and Protocol

(Section 5.1 is included as a modified version of [20] with permission)

This thesis will include examination and analysis of preliminary data collected from one human subject. This analysis will help reinforce our understanding obtained from the simulations. The examination of human data is required to verify the signal processing techniques used for EMG amplitude estimation, torque and angle measurements. This analysis would provide us with information on the accuracy for estimating mechanical impedance on real world data, using our processing techniques.

One healthy subject (with no known neuro-musculo-skeletal deficits of the right shoulder, arm or hand) participated in one experimental session. Eight EMG electrodes were applied to their right arm. The skin above the investigated (biceps and triceps) muscles was cleaned with an alcohol wipe. An array of four EMG electrode-amplifiers was secured over each of the biceps and triceps muscles, midway between the elbow and the midpoint of the upper arm, centered on the muscle midline ([11], Fig. 3). The two contacts of each electrode-amplifier were oriented along the muscle's long axis, the presumed direction of action potential conduction. Each electrode-amplifier consisted of a pair of 8-mm diameter, stainless steel, hemispherical contacts separated by 10 mm (edge to edge). The distance between adjacent electrode-amplifiers was approximately 1.5 cm. A single ground reference electrode was gelled and secured over the acromion process (along the shoulder). Each electrode-amplifier had a gain of 20 and a common mode rejection ratio > 90 dB at 60 Hz. Each electrode-amplifier signal was eighth-order

(15 Hz) high-pass filtered, amplified (selectable gain), electrically isolated and fourth-order (1800 Hz) low-pass filtered.

The subject was seated and secured into the experimental apparatus (Figure 5-1). Their right upper arm was positioned in a plane parallel to the floor and forearm in the same plane but at 90^o to the upper arm (shoulder abducted 90^o from the anatomic position). The forearm was oriented in the parasagittal plane, with elbow flexed 90^o. The subject's right wrist was rigidly attached to the manipulandum with a cuff at the styloid process (Figure 5-2). The subject was instructed to relax all muscles not directly involved in the task, and to maintain a consistent posture and contraction technique throughout all trials. The subjects was first encouraged to perform MVCs (separately for flexion and extension) by slowly increasing torque (over 2–3 s) until MVC was reached, and to maintain MVC for a 3 second recording. The average torque from the average of two such trials was used as the MVC. Similarly, the average EMG amplitude from the average of two such trials was used as the maximum voluntary EMG (MVE). These simple MVC and MVE measures were sufficient to evaluate torque over a modest range for each subject. The subject was provided a three minute rest between these, and subsequent contractions, so as to prevent neuromuscular fatigue. Subjects were released from the cast restraint between trials to ensure normal circulation in the periphery.

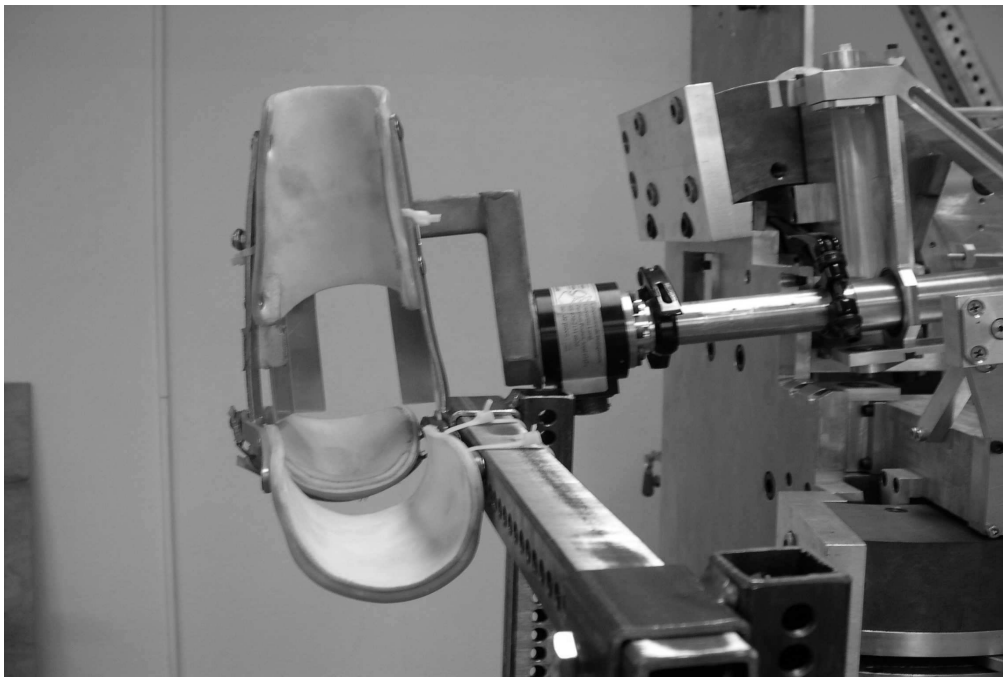

Figure 5-1 Experimatal set up of the robotic arm and the cuff where the subjects places his/her arm

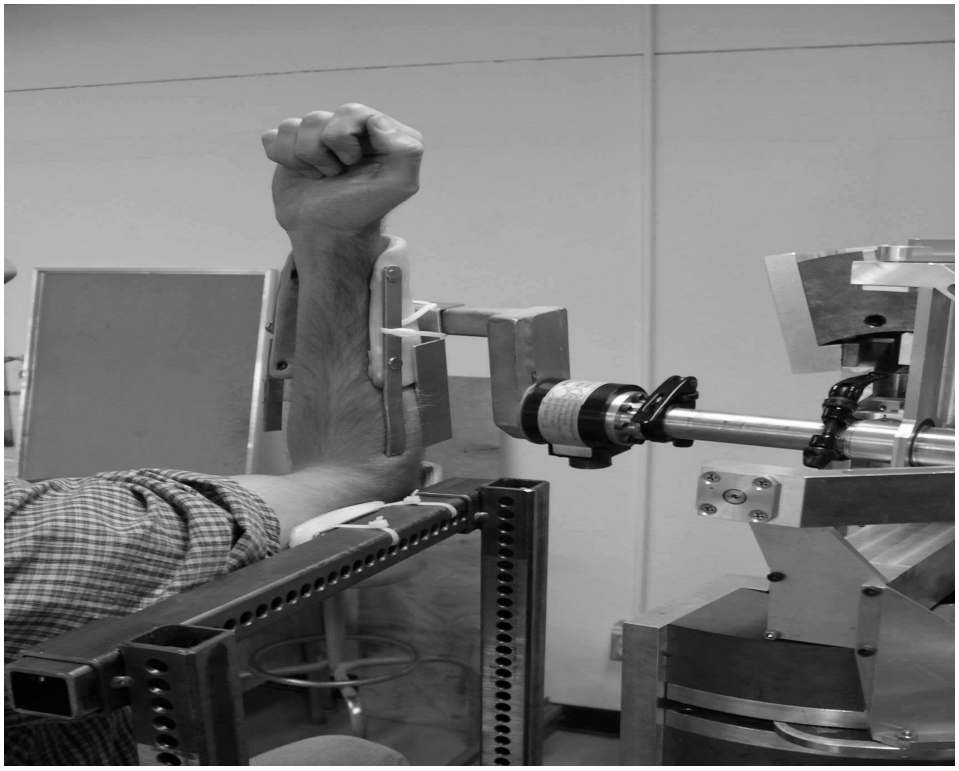

Figure 5-2 Subject seated in the experimental apparatus with his right arm placed in the manipulandum

The subject next produced a series of contractions necessary for calibrating EMG-amplitude estimation algorithms and EMG-torque modeling. In this section of the experiment, the actuator was locked in place at 90^{o} elbow angle (fixed position, so that only the torque measurement is relevant) and the feedback PC displayed only a target torque and the achieved torque. First, EMG was recorded for 5 seconds while subjects completely relaxed their muscles (0% MVC; with the subject's arm removed from the manipulandum). Second, two 50% MVC constant-force contractions were recorded for each of attempted flexion and extension. Subjects were instructed to begin at rest, and then gradually (over a duration of 2–3 s) increase effort until the target torque level is maintained. At this time, a 5 s recording was made. These first two contraction sets are sufficient for calibration of the advanced EMG amplitude estimation algorithms [11].

Third, the target torque level was ramped from 50% MVC extension to 50% MVC flexion in 30 seconds. Recordings were made while subjects completed two of these slow ramp contractions. Fourth, the unperturbed torque ramp contractions were repeated, but this time the ramp was extend from 50% MVC flexion to 50% MVC extension. Contraction sets three and four provided the data necessary for EMG-torque modeling during quasi-static conditions [3]. Fifth, the target torque level was modulated in a random fashion between 50% MVC flexion and 50% MVC extension [11]. The random target movement obeyed a uniform probability density function and was limited to a statistical bandwidth of 0.5 Hz [11]. The subject practiced target tracking, and once capable of adequately tracking, recorded for four 30 second trials. Contraction set five provided the data necessary for EMG-torque modeling during dynamic, constant-angle conditions [16].

Impedance measurements were next acquired. The joystick was set to obtain a nominal joint angle of 90º. Feedback consisted only of the target position and achieved position. An initial, constant target position was provided and the subject was asked to generate torque to match this position. The perturbations commenced. The subject was instructed to maintain the target torque level—on average—without resisting the perturbations, and with as little muscle co-contraction as possible. A 30 s recording was then made. This procedure was repeated until two recordings each had been made at target torque levels of 10%, 25% and 40% MVC extension and flexion. These constant-torque recordings allowed replication of prior impedance measurement trials and formed discrete points relating EMG to impedance. Next, the target torque level was ramped from 50% MVC extension to 50% MVC flexion in 30 s, while perturbations were applied.

Again the subject was instructed to follow the target position—on average—without resisting the perturbations, and with as little muscle co-contraction as possible. Once the subject was able to adequately follow the target, the 30s trial was recorded. Four such trials were recorded during extension to flexion contraction, and four trials during flexion to extension contraction. These slowly force-varying trials were used to develop the EMG-impedance models.

5.2 Analysis of Experimental data

5.2.1 Constant torque trials

We have presented here an analysis of the data collected from one particular subject. Data were collected using the procedure in section 5.1. The data were then processed using techniques developed from our simulation studies. Signal processing techniques were run on the collected data and their results were analyzed. Data from the constant torque bias experiments were first processed to verify that the data coincided with experiments conducted by previous researchers. Figure 5-3 shows the total torque measured for six different experiments. Each experiment was conducted at a particular bias torque as mentioned on top of each plot. Figure 5-4 shows a plot of the ΔTorque values after subtracting out the torque bias (mean torque level) from the total torque measurements.

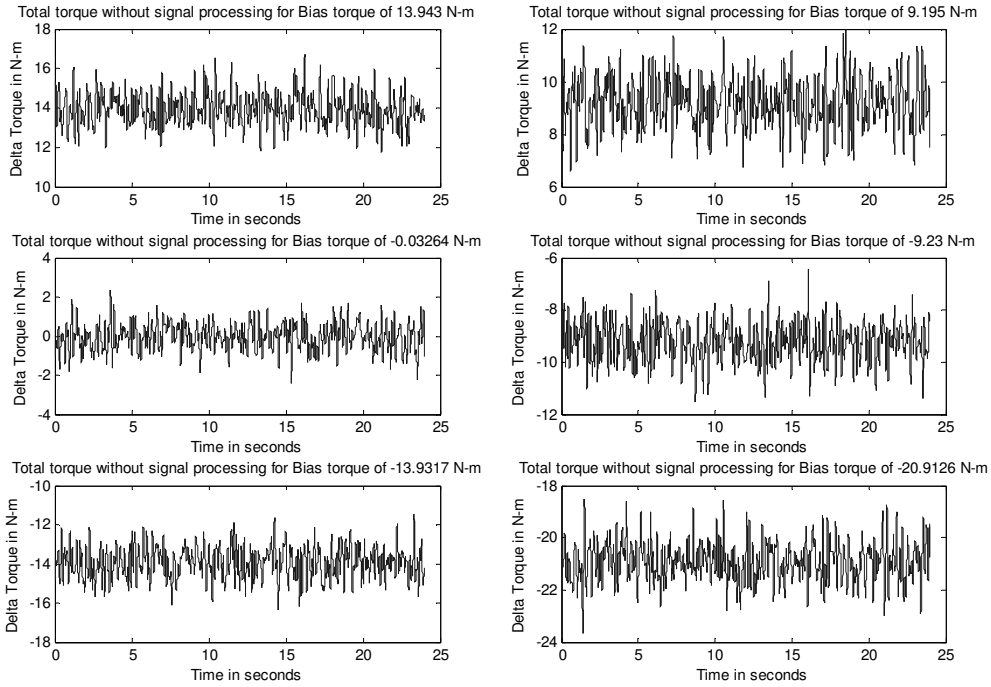

Figure 5-3 Total torques measured for constant torque bias trials (trial nos. 13-18) with background torques as mentioned (13.94N-m, 9.195N-m, 0N-m, -9.23 N-m, -13.9317N-m and -20.9125N-m).

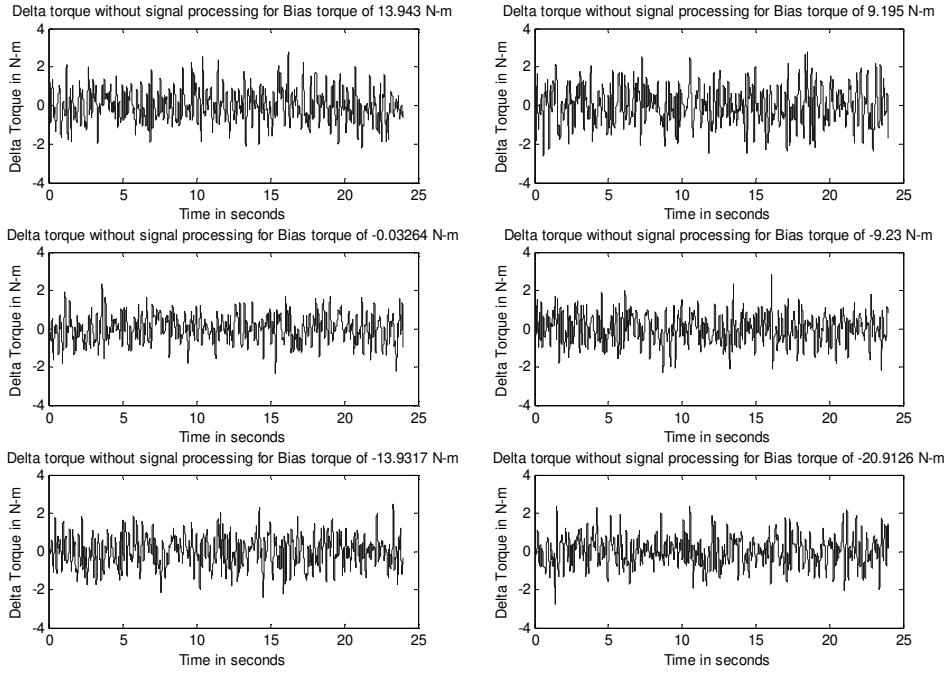

Figure 5-4 Delta torques for various constant torque bias trials, after removing the background torques from total torque measurements.

The plots in Figure 5-5 show the angular deviations recorded for the corresponding experiments. For the purpose of analysis, let us consider three (bias torques of 13.943 N-m, 0 N-m and -20.9126 N-m) of the six experiments here in detail. The ΔTorque plots (Figure 5-4) for these cases seem to be similar. Since the ΔTorque plots are similar and the bias torque is varying, we would expect the angular deviations to be varying.

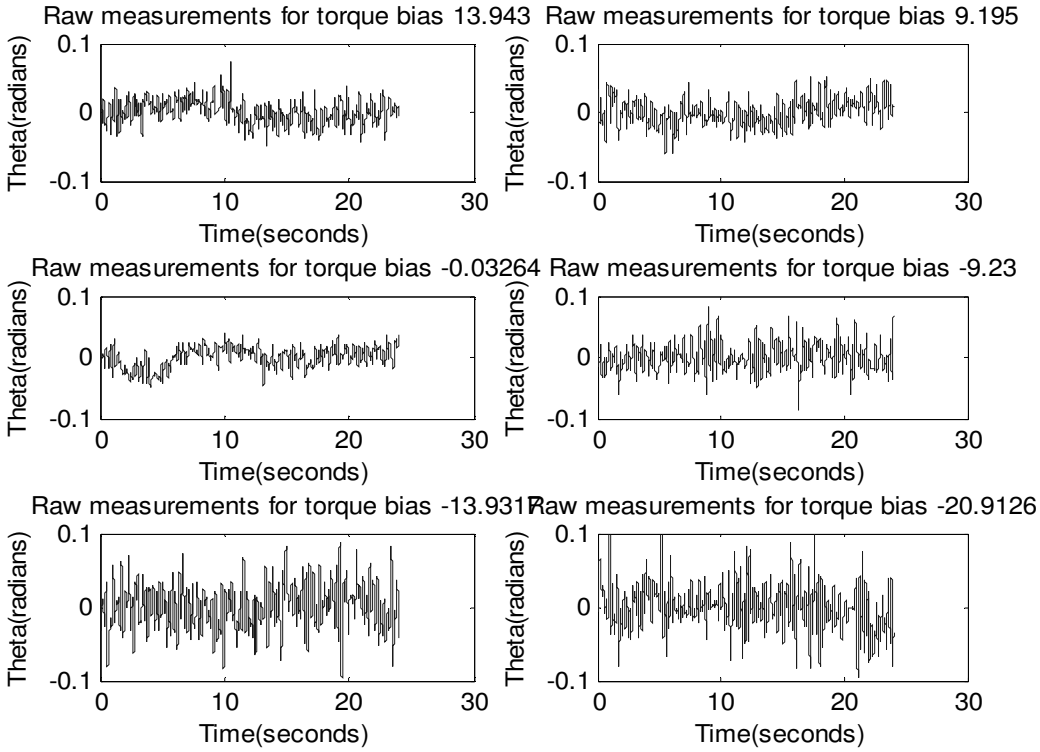

Figure 5-5 Measured angular deviations for constant torque bias trials.

A transfer function plot is needed to evaluate the data collected. The plots would help verify results produced by previous researchers. Figure 5-6 shows a plot of the transfer function $\frac{\Delta\theta}{\Delta T}$ for trial no.15 (torque bias of 0 N-m). The angular deviations and the torque have not been processed, i.e., the low frequency artifacts, shown in Figure 5-5, has not been removed. Note that there is a low frequency drift associated with the angular

deviation measurements, which have to be removed by estimating the best fit polynomial. The torque signal is the input signal from the computer and therefore there is no low frequency drift associated with the torque. However, the mean torque has to be subtracted out to obtain ΔT . The motor used to perturb the subject, has a bandwidth of only about 15 Hz. Any information above this frequency would be noise in the torque measurements. Figure 5-6 shows the transfer function obtained. The information above 10 Hz is corrupted by the limited motor bandwidth and the information below 2-3 Hz is corrupted due to the drift in the angular measurements. The remaining spectrum is characteristic of a second-order system. The unnecessary portions of the signal have to be removed from the measurements.

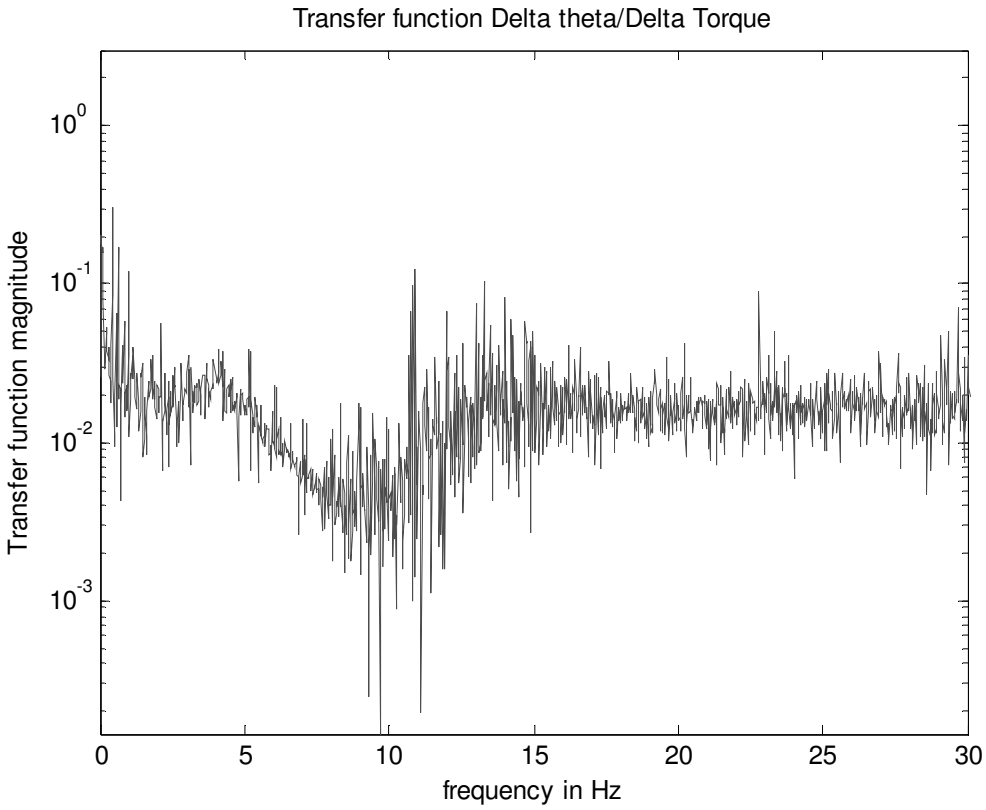

Figure 5-6 Transfer function $\frac{\Delta\theta}{\Delta T}$ for trial no.15 (background torque of 0 N-m) without signal processing the data

The torque and the angular measurements were next processed and the transfer function again plotted. The low frequency drift in the angular deviations was removed by subtracting a 14th degree polynomial. Various degree polynomials were tried and visually assessed with respect to their fit to the total torque. A higher order polynomial would fit to the Delta_T signal itself and not the low frequency content while a low order polynomial would not be able to remove the low frequency component. The decision of using a 14th degree polynomial was qualitative, after observing the polynomial fit. Figure 5-7 shows a plot of the angular measurements (θ) and the 14th degree polynomial

(smooth line running through the plot). This polynomial is subtracted out from the angular measurements to get the change in angle ($\Delta\theta$) as in the bottom plot Figure 5-7. The ΔT and $\Delta\theta$ were then 10 Hz low-pass filtered using a FIR filter because the motor was capable of a maximum of 15 Hz perturbations. Data greater than 15 Hz is not useful for system identification. Figure 5-6 shows that the transfer function plot starts to rise back at a frequency of about 10 Hz. Therefore it was decided to have the low pass cut-off at 10 Hz.

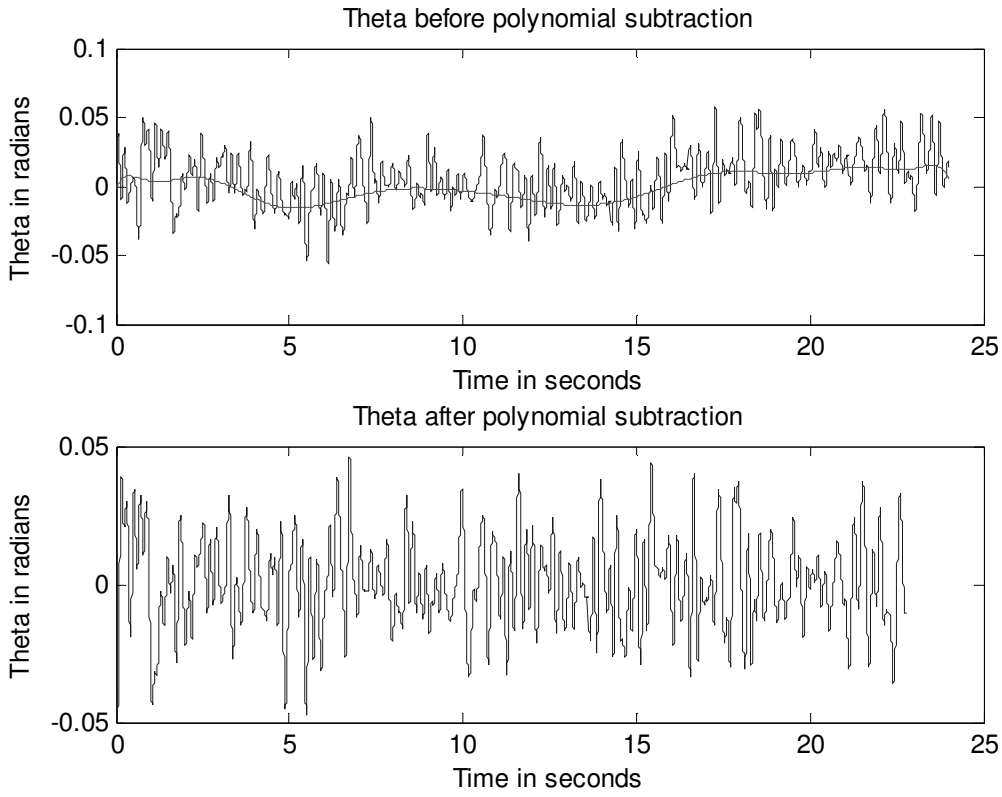

Figure 5-7 Polynomial subtraction from angular deviations to remove the slowly varying bias. The top plot represents the angular deviations data and the best fit polynomial(14th degree) (solid line) running through the plot. Bottom plot represents the angular deviations after subtracting the polynomial.

The transfer function $\frac{\Delta\theta(f)}{\Delta T(f)}$ is now plotted after performing the above signal processing methods. This plot can be observed in Figure 5-8. The smooth line through the

plot represents the transfer function obtained using the parametric approach. K, B and I were estimated (after filtering of $\Delta\theta$ and ΔT) using linear least squares (as explained in 4.1.5) using Equation 4-1. The smooth line represents the line $\frac{1}{K + Bs + Is^2}$

where $s = j*2*pi*f$, f being the frequency in Hz.

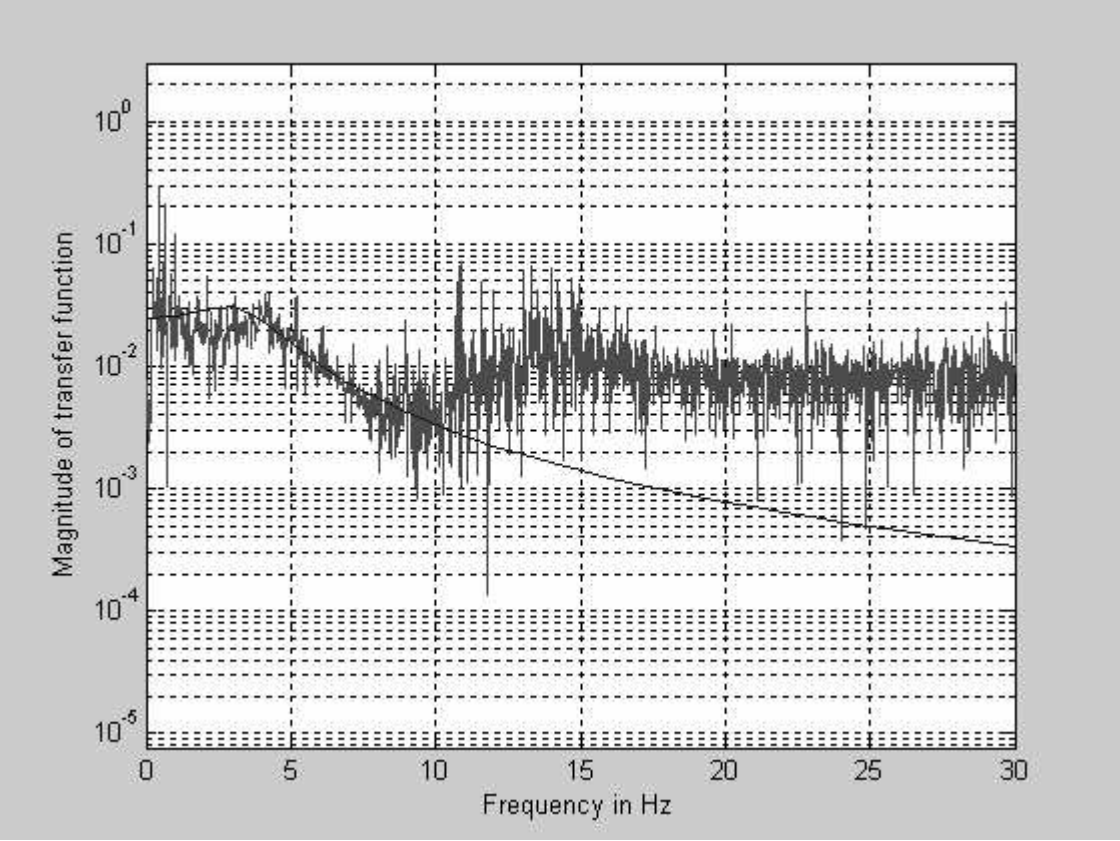

Figure 5-8 Transfer function $\frac{\Delta\theta}{\Delta T}$ for trial no.15 (background torque of 0 N-m) after polynomial subtraction and low pass filtering (10 Hz) of angular measurements. The smooth line represents the second order curve got from the parametric approach after estimating the K, B and I parameters.

The results of the parametric approach and the non-parametric approach match up well between the frequencies of 2 -10 Hz. The transfer function plot of the non-parametric approach rises after 10 Hz. Note that the above parametric approach has not used EMG data for estimating K, B and I.

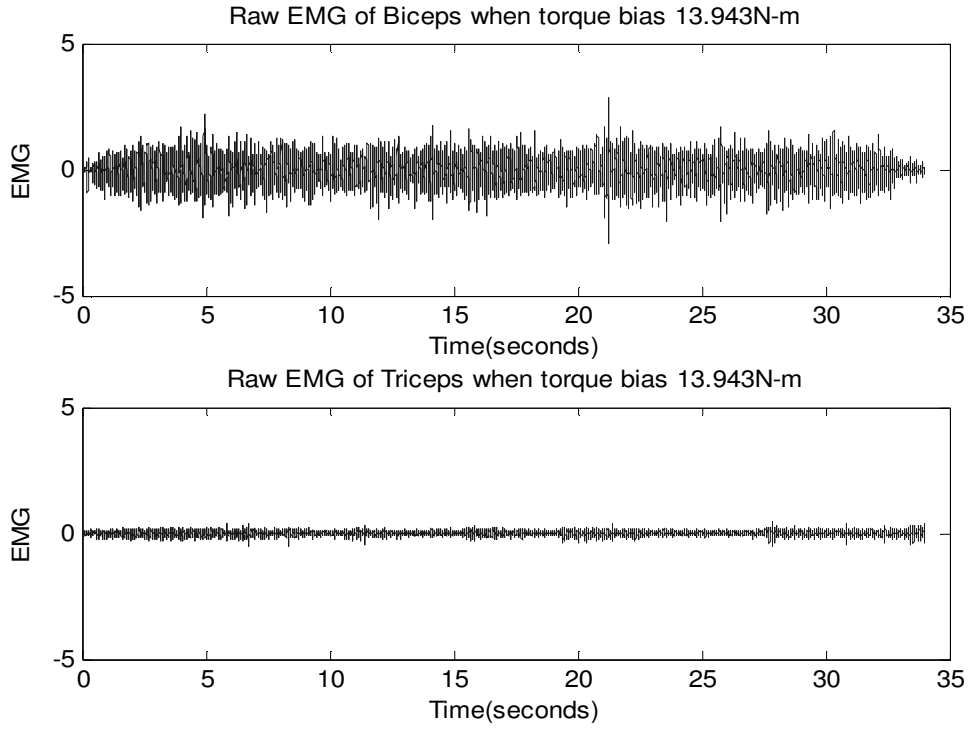

Figure 5-9 EMG activity (in volts) seen in the biceps and triceps for background torque of 13.943 N-m over a period of 35 seconds..

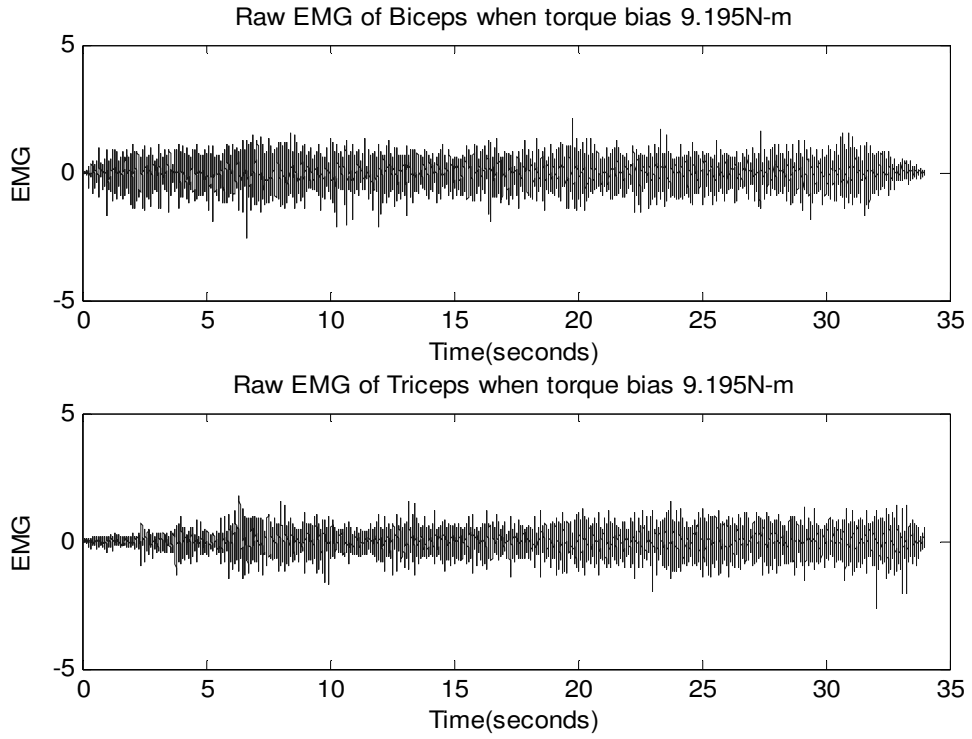

Figure 5-10 EMG activity (in volts) seen in the biceps and triceps for background torque of 9.195 N-m .

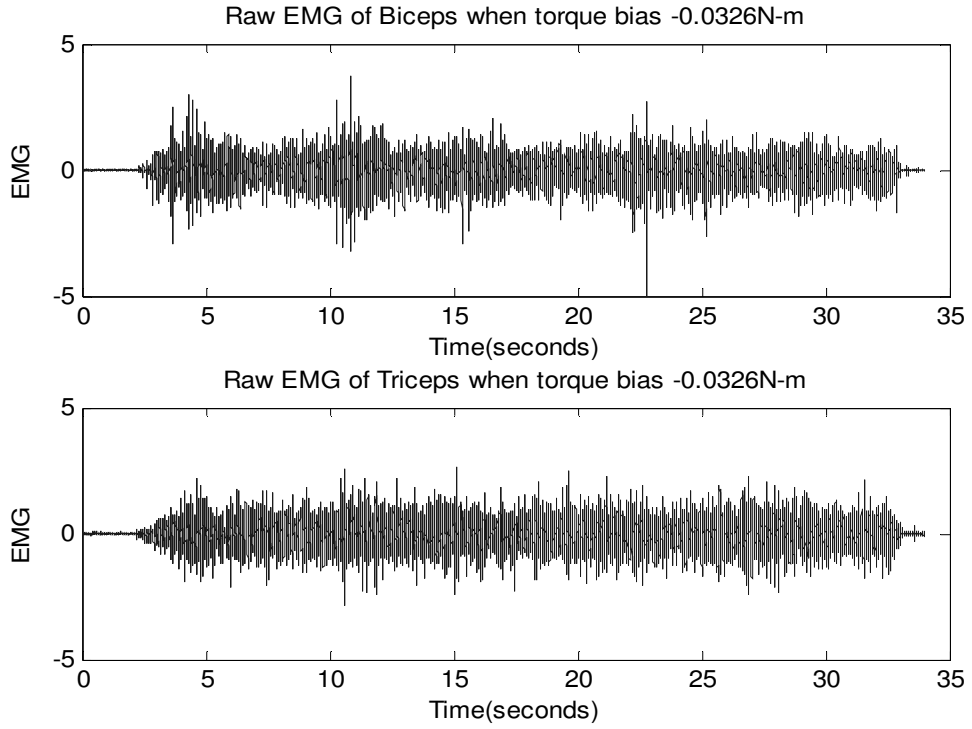

Figure 5-11 EMG activity (in volts) seen in the biceps and triceps for background torque of 0 (approx) N-m

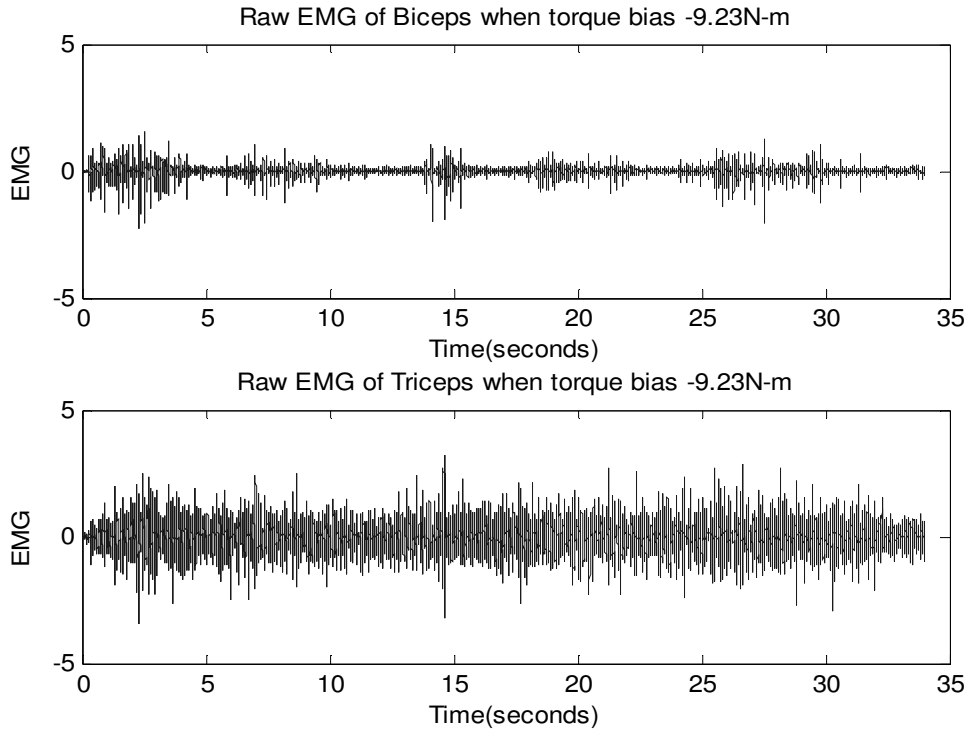

Figure 5-12 EMG activity (in volts) seen in the biceps and triceps for background torque of -9.23 N-m

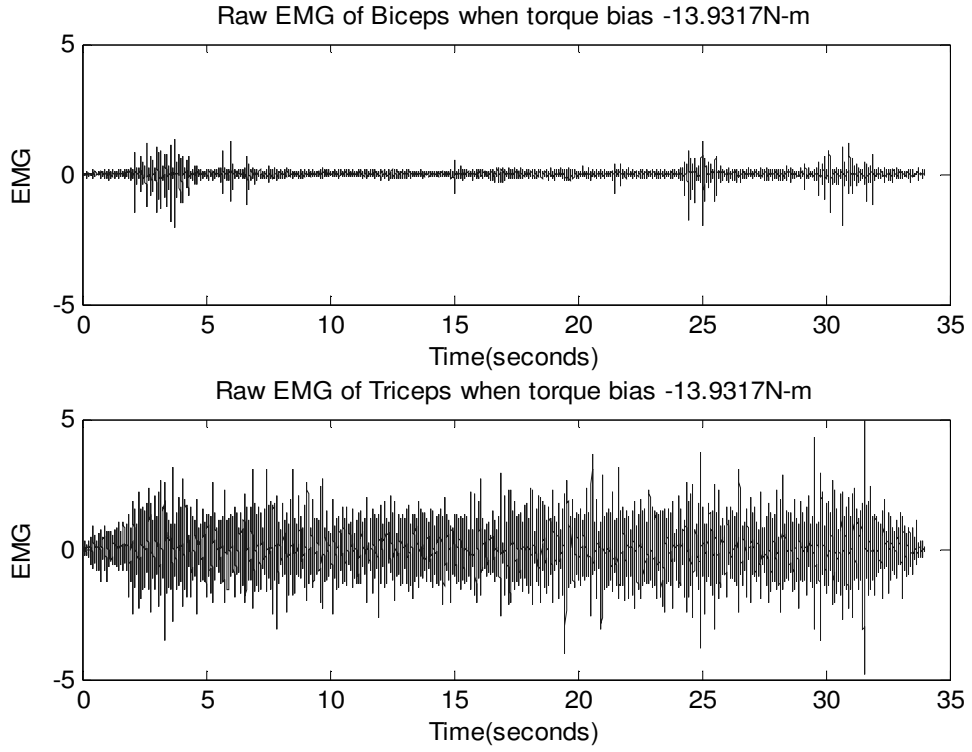

Figure 5-13 EMG activity (in volts) seen in the biceps and triceps for background torque of -13.93 N-m

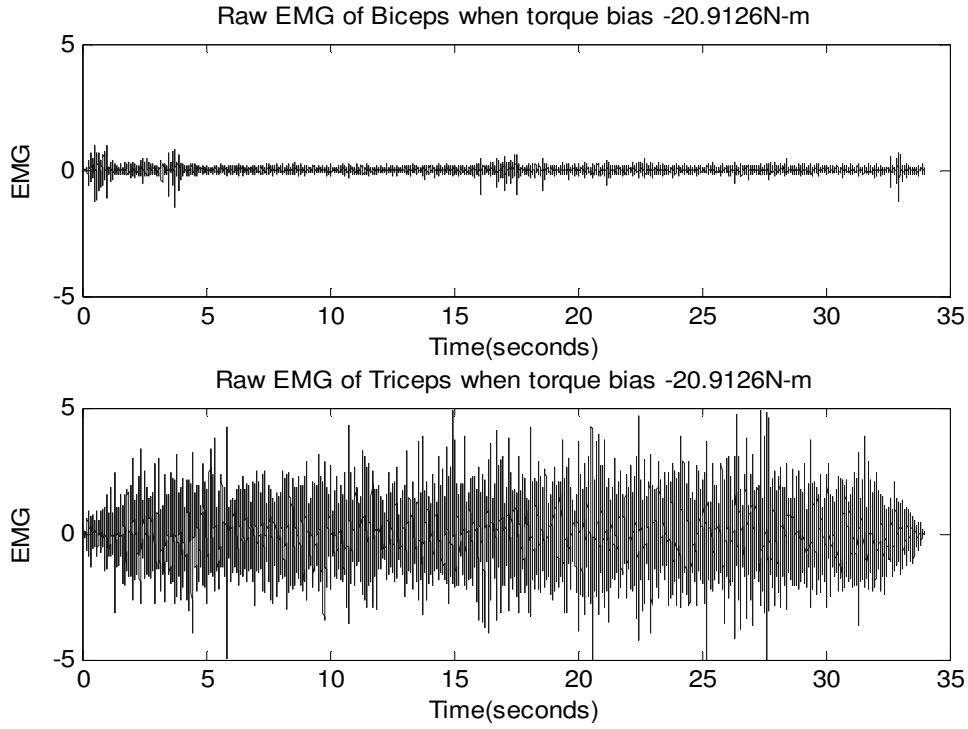

Figure 5-14 EMG activity (in volts) seen in the biceps and triceps for background torque of -20.9126 N-m.

The EMG activity in the biceps and triceps, for different background torques can be seen in Figure 5-9 to Figure 5-14. For each of those plots, recordings from four channels were collected for each muscle group (biceps/triceps). We have picked one channel per muscle to be representative of the muscle. The estimates of the impedance parameters for various trials are shown in Figure 5-15. For the purpose of analysis, trials corresponding to background torques of 13.94 N-m (Figure 5-9 for EMG activity), 0 N-m (Figure 5-11 shows EMG activity) and -20 N-m (Figure 5-14 shows EMG activity) will be considered in detail.

The ΔT plots (Figure 5-4) for trials with different torque bias seem to be the same, as desired by the experimental protocol. Since ΔT is same and the background torque for the trials are varying, the change in angular deviations would be expected to vary. Higher background torques would be accompanied with higher values of K and B

and a lesser change in angular deviation. The values of K and B would be expected to be near zero at a torque bias of 0 N-m and would be expected to be larger for -20 N-m and 13 N-m. However, this pattern is contrary to what is observed in the plot of Figure 5-15 where the values of K and B are higher at 0 N-m torque bias than -20 N-m. We can see from Figure 5-5 that $\Delta\theta$ (change in angular deviation) is greater for 0 N-m than -20 N-m. The reason for this result can be attributed to the co-contraction at 0 N-m as can be seen from the EMG data shown in Figure 5-11. The subject co-contracted their arm resisting motion at 0 N-m. The inertial parameter (I) does not change appreciably over the experiments as has been seen by previous researchers.

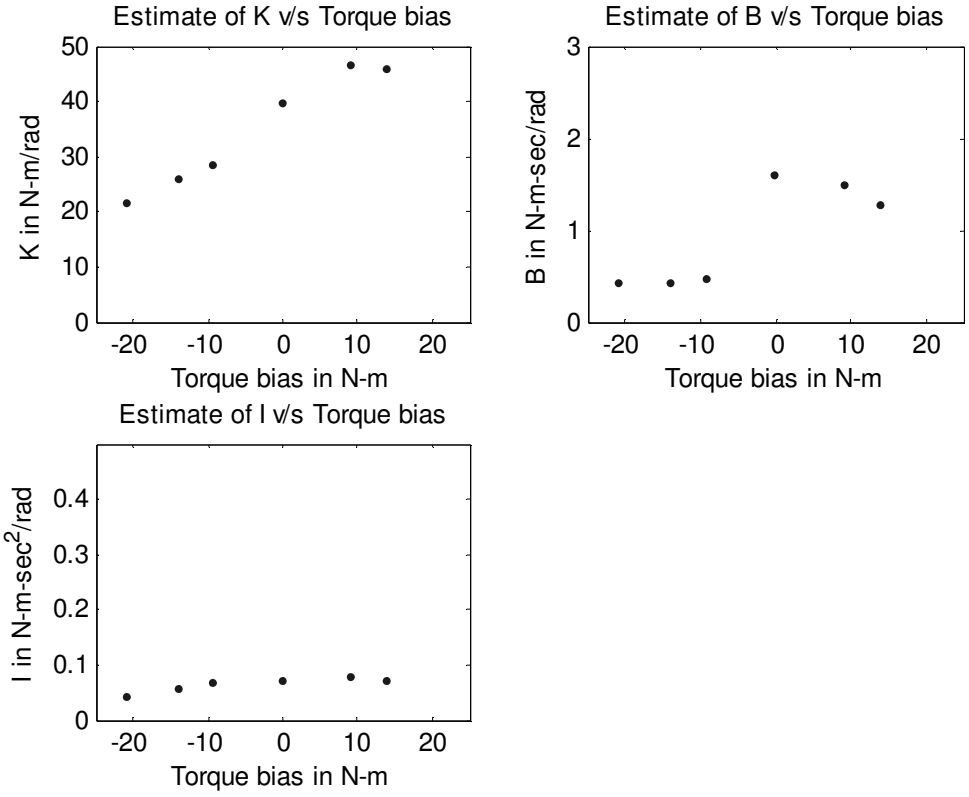

Figure 5-15 Estimate of K, B and I v/s the torque bias

5.2.2 Ramp Contractions

The next experiment consisted of background torque varying as a ramp. Figure 5-16 shows the total torque measurement for one of the four different trials and Figure 5-17 displays the corresponding angular deviations. Figure 5-18 show plots of the EMG activity (four channels were used to record each muscle group but we have shown only one channel as being representative of the muscle) during the experiment. Figure 5-19 and Figure 5-20 give the estimates of K and B with respect to time. Parameters $ke, kf, be \text{ and } bf$ were first estimated using EMG amplitudes by linear least squares (as in section 4.5). K and B were then calculated using $ke, kf, be \text{ and } bf$ (using Equation 4-7 and Equation 4-8).

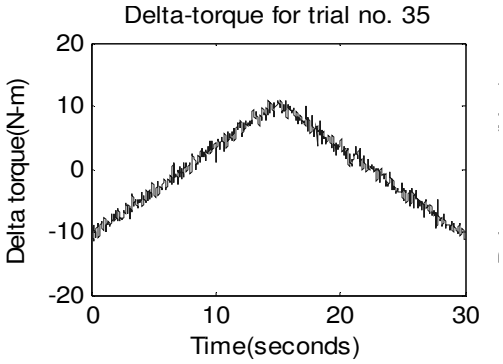

Figure 5-16 Total torque measurements of an experiment with background torque varying as a ramp.

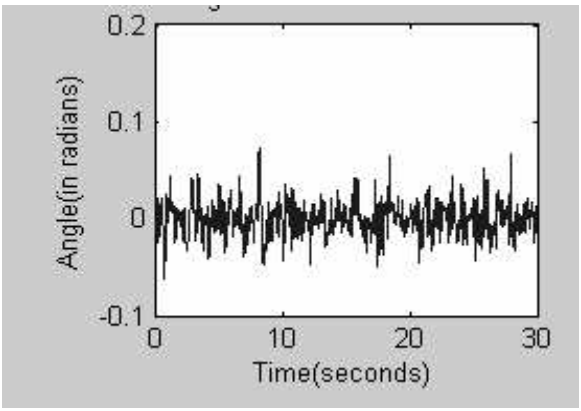

Figure 5-17 Angular measurements (in radians) for trial no.35 .

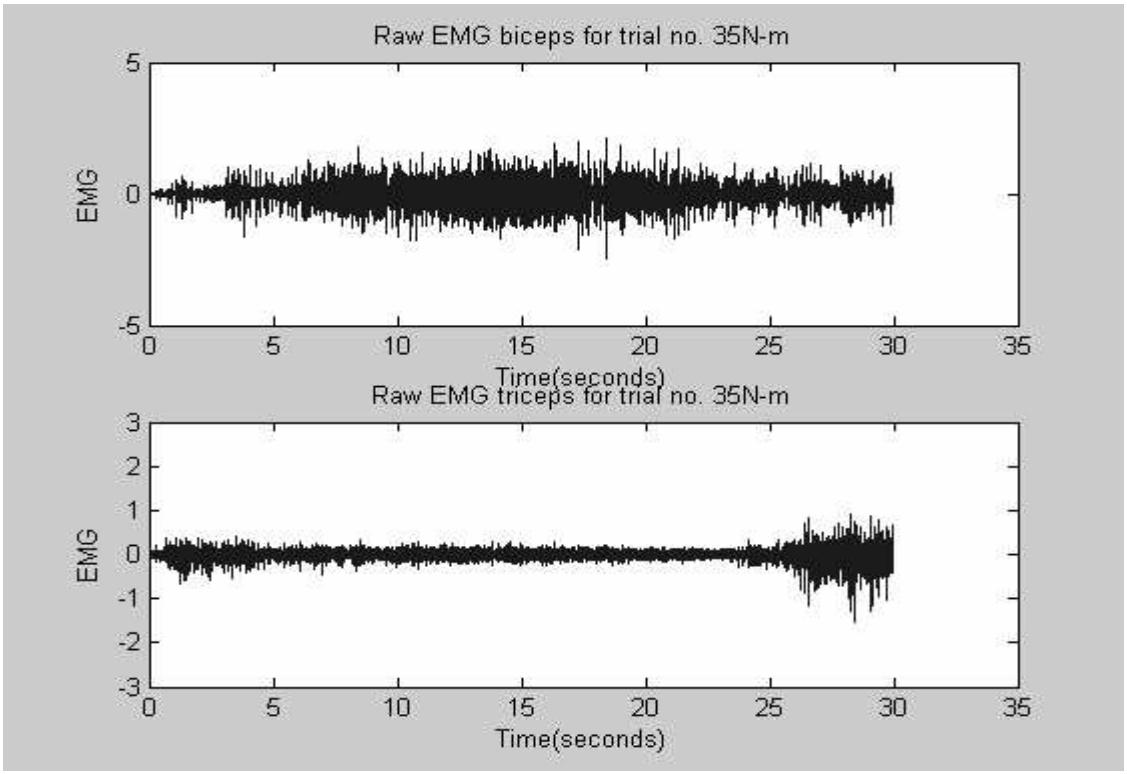

Figure 5-18 EMG activity in the biceps (top plot) and triceps (bottom plot) for trial no.35.

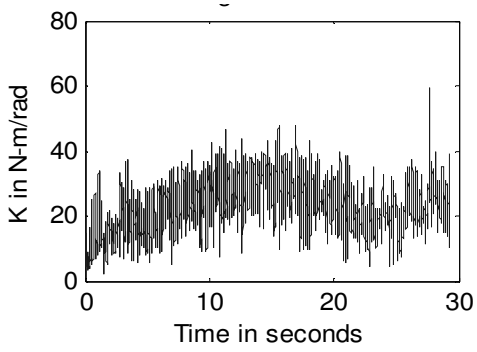

Figure 5-19 Estimate of elastic parameter K with respect to time.

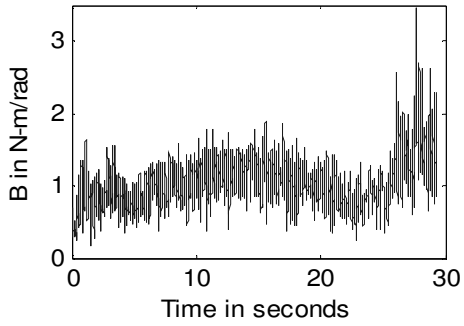

Figure 5-20 Estimate of elastic parameter B with respect to time.

The torque bias (Figure 5-16) varies from -10 N-m to 10 N-m in the first 15 seconds and then 10 N-m to -10 N-m in the next 15 seconds. The change in torque (ΔT) about the bias torque is about the same for the length of the experiment. Since the bias torque is changing and the ΔT is about the same, the angular deviations would be expected to change during the experiment but this is not clear with the data that we have in Figure 5-17. The EMG activity in Figure 5-18 shows that the biceps are predominant during the experiment and there is some amount of co-contraction during the last five seconds of the 30 second duration.

The impedance estimate K (from Figure 5-19) shows that there is a slight increase in the value of K up to 15 seconds and then reduces from 15 to 28 seconds. Towards the end, there is an increase in value of K, and this could be attributed to the muscle co-contraction seen towards the end of the experiment. The change in value of K over time

can be compared with the muscle activity in the biceps since it is not as visible in the angular measurements. The activity of the biceps tends to increase until 15 seconds and then later reduces. The result of this change is the estimate of K gradually increasing and then falling off after 15 seconds, before it rises again due to muscle co-contraction.

This preliminary examination of data would be of help for future experiments. It has been understood that co-contraction during experiments could lead to estimates that are not consistent with the literature. The subject needs to be instructed about relaxing during zero torque bias conditions. The angular deviations are associated with a low frequency component which could be removed by subtracting out a polynomial. A 14^{th} degree polynomial worked well for this set of data. The motor is not capable of producing perturbations greater than 15 Hz. Therefore, all the data including $\Delta\theta$, $\Delta\dot{\theta}$ and $\Delta\ddot{\theta}$ are low pass filtered at 15 Hz.

6 Conclusions and Future work

6.1 Conclusions and Discussion

The objective of this project was to perform simulations prior to conducting a pilot experiment with associated data analysis. The simulations helped to provide insight into conducting the experiment. Various schemes were attempted to overcome the problem of slowly varying drift with the torque measurements. Subtracting out a polynomial was the best among them. The angular measurements, in the real data analysis, had a slowly varying component. A 14^{th} degree polynomial was subtracted out from the angular measurements to remove this component. A 14^{th} degree polynomial worked best since a

higher degree polynomial would fit to the data itself rather than the drift, and a lower degree polynomial would not be sufficient to remove the drift.

Simulations also helped us understand the length of data that need be collected for proper system identification, for the case of estimating impedance using EMG for this second-order model. The noise in EMG amplitudes and the length of data were varied to find out the optimal length of data required. Thirty seconds of data for EMG amplitude estimates of SNR 15 resulted in impedance estimation errors under 5%.

Physical data from one subject were collected and the techniques learned from simulation were applied on them. The ΔT and $\Delta\theta$ signals were low pass filtered at 10 Hz before obtaining the 2nd order transfer function $\frac{\Delta\theta}{\Delta T}$. This non-parametric approach was compared against the parametric approach (Figure 5-8). Co-contraction during experiments caused high impedance at torque bias of 0 N-m which would otherwise be expected to be zero. The impedance estimates were compared with raw EMG and angular deviations to check for validity of the estimates. The ramp torque bias trials showed that the range of values over which K and B changed were low. This result was due to the fact that when the biceps relaxed, the triceps contracted and vice versa. Further, there were not appreciable changes in $\Delta\theta$. The subject's contraction pattern would need to be altered by a different set of instructions or by altering the background torque target.

6.2 Suggestions for future work

Data were collected from one subject as preliminary data examination. It would be necessary to collect data from more subjects to be able to verify our signal processing techniques and also to be able to understand the experiments involving ramp contractions. The subjects would need to be trained and instructed to avoid co-contraction, both during the constant torque bias trials and the slowly varying torque bias trials. Co- contraction by subjects, during experiments, was a reason for K and B not varying over a sufficient range. Therefore, the EMG-impedance relation could not be evaluated over a range of conditions.

A first degree polynomial relation was assumed for the relation between EMG – stiffness (Equation 4-7) and EMG – viscosity (Equation 4-8). Higher degree polynomial relationships can be used and their performance can be evaluated. The motor used for perturbations had a maximum capacity of 15 Hz. Therefore, low-pass filters of 15 Hz had to be used to remove any data greater then 15 Hz. This process results in losing high frequency content, which could otherwise be used for system identification. It would be helpful to use a more powerful motor with a greater capability.

7 References

1. Loeb G E and Gans C “Electromyography for Experimentalists” The University of Chicago Press, 1986.
2. “Selected topics in surface electromyography for use in the occupational setting : Expert perspectives” U S Department of Health and Human services National institute for occupational safety and health . March 1992.
3. Clancy EA, Hogan N. Relating agonist-antagonist Electromyograms to joint torque during isometric, quasi isotonic non-fatiguing contractions. IEEE Trans Biomedical Eng 44(10):1024-1028, 1997.
4. I W Hunter and R E Kearney Dynamics of human ankle stiffness: variation with mean ankle torque. Journal of Biomechanics, 1982.
5. Robert E. Kearney and Ian W. Hunter, System identification of Human joint dynamics.Critical reviews in Biomedical Engineering. Vol 18 issue1 1990.
6. Basmajian,J.V And De Luca,C.J. Muscles Alive (fifth edition). Baltimore: Williams and Wilkins,1985.
7. I W Hunter and R E Kearney “Dynamics of Human Ankle stiffness: variation with mean ankle torque” Journal of Biomechanics vol 15 No10 1982.
8. Osu R, Kamimura N, Iwasaki H, Nakano E, Harris CM, Wada Y, Kawato M Optimal impedance control for task achievement in the presence of signal-dependent noise. Journal of Neurophysiology, 1199-1215, 2004, 1992.

9. Osu.R, Gomi. H Multi-joint Muscle regulation mechanisms examined by measured human arm stiffness and EMG signals. Journal of Neurophysiology 81:1458-68,1999.
10. Osu R, Franklin DW, Kato H, Gomi H, Domen K, Yoshiaka T, Kawato M.Short and long term changes in joint co-contraction associated with motor learning as revealed from surface EMG. Journal of Neurophysiology 88:991-1004, 2002.
11. Clancy, Edward A. and Farry, Kristin A., "Adaptive Whitening of the Electromyogram to Improve Amplitude estimation", IEEE transactions on Biomedical Engineering, Vol. 47, No. 6, June 2000.
12. William Press, Saul Teukolsky, William Vetterling. Numerical Recipes in C (pg 671-pg680).Second edition, Cambridge University press, 1992.
13. Zhang Q and Rymer W Z, Simultaneous and non linear identification of mechanical and reflex properties of human elbow joint muscles. IEEE transactions on Biomedical engineering Vol 44,No 12, Dec 1997.
14. Yves St-Amant, Denis Rancourt and Edward A. Clancy. Influence of Smoothing window length on Electromyogram estimates. IEEE transactions on Biomedical Engineering vol 45, No 6 June 1998.
15. Yves St-Amant, Denis Rancourt and Edward A Clancy, Effect of Smoothing window length on RMS EMG amplitude Estimates. IEEE Bio-engineering conference 1996.
16. Clancy EA, Bouchard S, Rancourt D. Estimation and application of Electromyogram (EMG) amplitude during dynamic contractions. IEEE Eng Med Biol Magazine vol 20:47–54, 2001.

17. Proakis JohnG, Manolakis Dimitris G. Digital signal processing: principles, algorithms, and applications. Second edition Maxwell Macmillan International, 1992.
18. MATLAB help pages for filtfilt, The Mathworks, Natick, MA. http://www.mathworks.com/.
19. Sherwood, Lauralee Human Physiology from cells to systems fifth edition. Thomson Brooks/Cole.
20. Edward A. Clancy, Grant application to the Department of Health and Human Services, 2002.